Effects of nonlinear noise reduction algorithms on image quality in computed tomography systems

Evaluations using human observers and methods for assessing distortion

Joel Larsson

Department of Medical Radiation Sciences
Institute of Clinical Sciences
Sahlgrenska Academy
University of Gothenburg

Gothenburg, Sweden, 2022

UNIVERSITY OF
GOTHENBURG

Cover illustration by Joel Larsson

Effects of nonlinear noise reduction algorithms on image quality in computed tomography systems – Evaluations using human observers and methods for assessing distortion

joel.larsson@gu.se
joel.larsson@vgregion.se

ISBN 978-91-8069-007-2 (Print)
ISBN 978-91-8069-008-9 (PDF)
E-publication: http://hdl.handle.net/2077/72574

Printed in Borås, Sweden 2022
Stema Specialtryck AB

To my beloved family

'My son, eat thou honey, because it is good;
And the honeycomb, which is sweet to thy taste:
So shall the knowledge of wisdom be unto thy soul:
When thou hast found it, then there shall be a reward,
And thy expectation shall not be cut off.'

Proverbs 24:13-14 KJV

Cover Illustration by Joel Larsson

Abstract

Many conventional radiological examinations have during the past decades been replaced by examinations performed on computed tomography (CT) systems. One reason is that a CT system, in contrast to a conventional X-ray system, depicts slices of the body so that anatomical structures to a lesser extent risk to obscure the potential pathology. This extra diagnostic information may increase the absorbed dose for patients, because the noise in CT examinations acquired at the same absorbed dose as conventional radiographs would have instead risked obscuring the pathology. Hence, if the noise in the CT images could be reduced by a mathematical algorithm a reduction in absorbed dose may also be possible. Traditionally, noise is reduced using linear convolution kernels, which weights the content of the CT image such that distinct variations are reduced. Concurrently, sharp edges in the image are smoothed out (the resolution is reduced), as sharp edges and noise are described by the same type of image content. Hence, the amount of noise reduction and consequently dose reduction will be limited by the required image resolution for the diagnostic task. In contrast to a linear algorithm, a nonlinear noise reduction algorithm is intended to reduce noise while keeping or increasing the image resolution. Hence, the image quality brought about by such an algorithm may depend on the content of the image including the noise level, which will make prediction of image quality in patients more difficult than for a linear algorithm. Further, nonlinear algorithms tend to distort the image. The impression of the image content may potentially be changed and aggravate the diagnostic assessment. Thus, the overall aim of the thesis was to investigate the effects of nonlinear noise reduction algorithms in CT imaging to help understand how to assess and predict image quality.

The nonlinear effect was investigated using human observer evaluation of paediatric cerebral and abdominal CT examinations, which had been noise reduced by a nonlinear noise reduction algorithm. However, for the abdominal examination, the combination effect of type of convolution kernel and noise reduction strength on image quality was investigated. These investigations showed the visualisation of some anatomical structure to increase, concurrently the resolution of other structures was shown to decrease as the strength of the noise reduction was increased. An edge-enhanced convolution kernel showed to compensate the reduced resolution. However, the visualisation of the structures was not found to be higher than the optimal strength of the noise reduction for the original convolution kernel.

The distortion effect was investigated using an objective method implemented from conventional radiography. The method showed that the tendency to distort the image content for the nonlinear algorithms increased with the noise level. However, the method does not visualize the distortion in the spatial domain. Hence, the method inspired to develop a new method, which shows where the distortion is located and how the image is distorted when noise is reduced by a nonlinear algorithm. The new method showed the distortion of the imaged object to be caused by the noise and the distortion of the noise to be caused by the imaged object.

The thesis emphasises the importance of investigating the distortion effect when nonlinear noise reduction algorithms are used to reduce the absorbed dose of CT examinations.

Keywords: Computed Tomography, Nonlinear noise reduction, Visual grading, Distortion analysis
ISBN 978-91-8069-007-2 (Print)
ISBN 978-91-8069-008-9 (PDF)
E-publication: http://hdl.handle.net/2077/72574

Populärvetenskaplig sammanfattning

Allt fler konventionella röntgenundersökningar har under de senaste årtiondena blivit ersatta av skiktröntgenundersökningar utförda på datortomografer. En orsak är att en datortomograf till skillnad från ett konventionellt röntgensystem avbildar skivor av kroppen så att organ i mindre grad riskerar att skymma eventuell sjukdom. Denna extra information om patientens kroppsliga tillstånd kan även öka stråldosen till patienten, eftersom bruset i en datortomografiundersökning utförd med samma stråldos som en konventionell i stället skulle kunna riskera att skymma det sjuka. Således är det möjligt att minska stråldosen om bruset i en datortomografibild kan minskas med hjälp av en matematisk algoritm. Det traditionella sättet att minska brus är att använda en linjär matematisk algoritm som viktar bildinnehållet på ett sådant sätt att distinkta förändringar i bilden minskas. Detta leder samtidigt till att skarpa kanter i bilden smetas ut (upplösningen blir lägre), eftersom skarpa kanter och brus beskrivs av samma typ av bildinnehåll. Därför blir mängden brusminskning och då även en stråldosminskning beroende på upplösningen som krävs för att kunna bestämma om patienten exempelvis är sjuk. Utöver linjära algoritmer, så finns det ickelinjära algoritmer avsedda att minska bruset medan upplösningen ökas eller förblir opåverkad. Kvaliteten på en bild framställd med en sådan algoritm blir beroende på vad som avbildats samt på brusnivån, vilket leder till att bildkvaliteten i en patient blir svårare att förutse än för en linjär algoritm. En ickelinjär brusminskande algoritm kan även tendera att förvränga bilden. Intrycket av bildinnehållet kan därför också möjligen ändras, vilket kan försvåra bedömningen av en sjukdomsfrågeställning. Därför var det övergripande målet med avhandlingen att studera effekten av ickelinjära brusminskande algoritmer vid datortomografibildtagning för att få hjälp att förstå hur bildkvalitet kan bedömas och förutses samt hur man kan genomföra en säker stråldosminskning för ett sådant system.

Den ickelinjära effekten studerades genom att röntgenläkare utvärderade datortomografiundersökningar av barns huvud och mage som brusminskats med en ickelinjär brusminskande algoritm. Vid magundersökningarna studerades även påverkan av att kombinera linjära med ickelinjära algoritmer. Dessa studier visade att vissa organ syntes bättre, men att upplösningen av vissa organ i kroppen blev lägre då graden av den ickelinjära brusminskningen ökades. Upplösningen visades i studien kunna kompenseras med en kantförstärkande linjär algoritm, men synbarheten av organen blev aldrig bättre än den mest optimala graden av den ickelinjära brusminskningen vid den ursprungliga linjära algoritmen.

Förvrängningseffekten studerades med hjälp av en matematisk metod som tidigare använts för att utvärdera ickelinjära brusminskande algoritmer vid konventionell röntgenbildtagning. Metoden visade att de ickelinjära algoritmerna tenderade att förvränga bildinnehållet mer då mängden brus ökade, men inte hur förvrängningen såg ut. Därför inspirerade denna metod till att utveckla en ny metod för datortomografi som visar var förvrängningen ägt rum och hur bilden förvrängts då bruset minskats med en ickelinjär algoritm. Den nya metoden visade att både det som avbildas och bruset kan förvrängas av varandra.

Avhandlingen understryker vikten att studera förvrängningseffekten då ickelinjära algoritmer avsedda att minska brus används för att minska stråldosen av datortomografiska undersökningar.

List of papers

This thesis is based on the following papers, referred to in the text by their Roman numerals.

I. Larsson J., Båth M., Ledenius K., Thilander-Klang A.

The effect of adaptive statistical iterative reconstruction on the assessment of diagnostic image quality and visualisation of anatomical structures in paediatric cerebral CT examinations

Radiation Protection Dosimetry 2016; 169(1-4): 115–122

II. Larsson J., Båth M., Ledenius K., Caisander H., Thilander-Klang A.

Assessment of clinical image quality in paediatric abdominal CT examinations – dependency on the level of adaptive statistical iterative reconstruction (ASiR) and the type of convolution kernel

Radiation Protection Dosimetry 2016; 169(1-4): 123–129

III. Larsson J., Båth M., Thilander-Klang A.

Frequency response and distortion properties of reconstruction algorithms in computed tomography

Radiation Protection Dosimetry 2021; 195(3-4): 416–425

IV. Larsson J., Båth M., Thilander-Klang A.

Visualization of the distortion induced by nonlinear noise reduction in computed tomography

Submitted

Contents

Abbreviations

AAPM	American Association of Physicists in Medicine
ART	Algebraic reconstruction technique
ASiR™	Adaptive statistical iterative reconstruction
CGLS	Conjugate gradient least-square
CNR	Contrast-to-noise ratio
CT	Computed tomography
$CTDI_{vol}$	Volume averaged computed tomography dose index
$CTDI_{w}$	Weighted computed tomography dose index
CUDA	Compute unified device architecture
d'	Detectability index
DI	Distortion index
ΣDI	Sum of distortion index
$\overline{DI}$	Mean of distortion index
DLP	Dose length product
DPS	Distortion power spectrum
DRL	Dose reference levels
FBP	Filtered back-projection
FOV	Field-of-view
GPU	Graphics processing unit
HU	Hounsfield unit
IRT	Iterative reconstruction technique
LCD	Liquid crystal display
MAR	Metal artefact reduction
MTF	Modulation transfer function
NI	Noise index
NPS	Noise power spectrum
NLD_{noise}	Nonlinear distortion of noise
NLD_{object}	Nonlinear distortion of objects
NLD'_{object}	Approximation of nonlinear distortion of objects
PA	Percentage of agreement
PFR	Principle frequency response
PMMA	Polymethyl methacrylate
PSF	Point spread function
RC	Relative concentration
ROI	Region of interest
RP	Relative position

RV	Relative rank variance
SFOV	Scan field-of-view
SIRT	Simultaneous iterative reconstruction technique
SNR	Signal-to-noise ratio
SSDE	Size-specific dose estimate
SSM	Strålsäkerhetsmyndigheten (Swedish Radiation Safety Authority)
TTF	Task transfer function
TV	Total variation
VG	Visual grading
ViewDEX	Viewer for digital evaluation of X-ray images

1. Introduction

1.1 Historical background

The discovery of X-rays in 1895 revolutionised the medical field by the introduction of radiological examinations. The physician was then enabled to detect pathology and diagnose patients by viewing X-ray images showing the internal organs. Although the interior of a patient was shown, the pathology might be obscured or concealed by overlapping anatomical structures, which might impair the possibility of making a correct diagnosis. However, the invention and installation of the first clinical computed tomography (CT) scanner in 1971 addressed the problem of overlapping anatomy, as this modality produced cross-sectional images through the reconstruction of several X-ray projections taken around the patient. The quote 'It looks exactly like the picture' from an enthusiastic surgeon, who was given the opportunity of viewing CT images of a patient with brain tumour before surgery,[1] may well describe the sensation of this new modality. Although tumours could be shown separated from anatomical structures by an early CT system, image quality was not always adequate to characterise the degree of severity.

The first CT system was exclusively designed for head examinations, as heart and respirational movement would have led to great inconsistency in the projection data using the acquisition technique at that time. The projection data of one CT image took approximately five minutes to acquire and five more for reconstruction. At that time, a full examination consisted of six images and was assumed to be completed in 35 minutes, as the reconstruction was processed during the scanning.[2] However, the increasing demand for CT examinations encouraged the development of innovations to speed up acquisition and reconstruction technique. The acquisition technique of the first CT system was sampling of the projection of each angle using a well-collimated X-ray (narrow) beam together with one detector that were translating over the patient. Current CT systems sample the projections using a fan-beam of X-rays that covers several rows of detector elements (Figure 1) and can acquire the projections from one rotation in less than 0.3 seconds. Consequently, reconstruction time had to follow the speed of the newer faster scans in order not to counteract the gained efficiency in workflow.

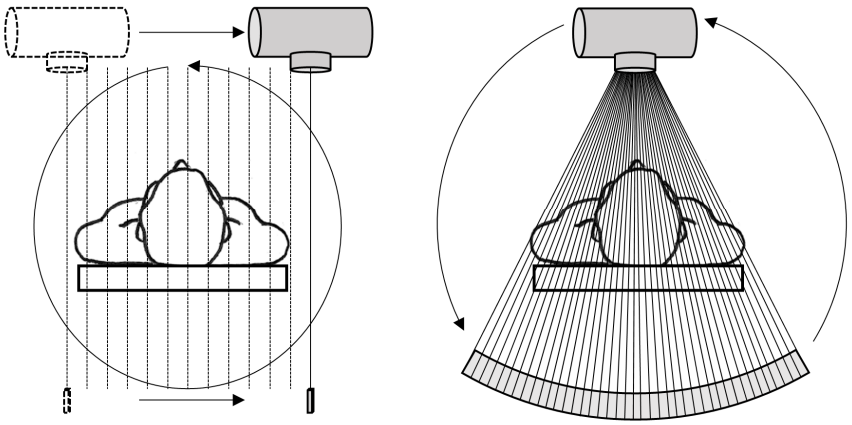

Figure 1. Illustration of the first-generation CT system where a well-collimated beam and detector are translated over the patient at each angle projection (left) and the most common third-generation CT system where the whole angle projection of the patient is covered at once by a diverging fan-beam (right). The third-generation CT system may achieve a rotation in under 0.3 seconds.

The improvements in hardware and acquisition procedure of CT systems also brought about higher image quality that further expanded the ability to diagnose patients in body parts other than the head and with other pathology referrals. Accordingly, the number of CT scanners in clinical use increased steadily in the UK (where the first clinical CT was installed), and in 1995 the number of CT scanners was 350 (166,000 people per CT scanner), while in Sweden the number was 115 (77,000 people per CT scanner).[3] Hence, the increased availability of CT examinations and more detailed diagnostic information has led to conversion of conventional X-ray examinations to corresponding CT examinations. Reports from the Swedish Radiation Safety Authority (SSM) estimated the annual number of CT examinations per 1,000 people to have increased from 39 in 1995, 72 in 2005, 98 in 2008 to 147 in 2018.[4–6]

X-ray examinations expose patients to ionising radiation and deliver an absorbed dose to the examined body part. Ionising radiation is associated with risk to an irradiated population and the atomic bomb survivors is a cohort well studied. The cohort has shown, among other things, that ionising radiation exposure increases the risk of cancer mortality throughout life and that the relative risk for cancer death is higher for those exposed at younger ages.[7,8] However, in risk estimations it is assumed that all the atomic bomb survivors received a whole body irradiation whereas in medical diagnostic X-ray examinations only a part of the body is irradiated. Further, the risk of low radiation doses is based on estimations using large populations such as the atomic bomb cohort. Hence, the risk associated

with an X-ray examination cannot be applied to specific patients. However, a reasonable conjecture is that the risk follows a relationship of linear non-threshold down to zero dose.[9] Consequently, optimisation aiming at minimising the radiation dose at a reasonable image quality is necessary. According to Swedish regulations, medical examinations have to be optimised according to image quality and radiation dose[10] and the exposure has to be performed with care especially when the patient is a child. Although, as long as the patient benefits from the examination, there is no dose limit for the medical exposure of the patient.[11] However, national dose reference revels (DRLs) are used as guidelines of reasonable radiation dose levels for specified diagnostic X-ray examinations[10]. Today in Sweden, DRLs for children (15 years-old and younger) are only set for cerebral and abdominal CT examinations, respectively. Further, the DRLs can indicate if for example the radiation dose for an CT examination is high or low. However, a radiation dose should not be lowered to the DRL if the CT system is not capable of generating a reasonable image quality at that dose. To achieve a dose reduction of a CT system, noise reduction techniques has been identified as having an important part to play.[12]

The first reconstruction technique used clinically in CT systems, the Algebraic Reconstruction Technique (ART), is a type of iterative reconstruction technique (IRT).[13] The reconstruction procedure of ART uses a system of equations related to all X-ray paths, at all acquired angles, and a summation of the signal to the detector element (ray-sum) for each corresponding path. The path is a given straight line from the X-ray focal spot to a detector element. Pixels (picture elements) which will form the reconstructed image are updated iteratively at every projection angle by comparing all measured ray-sums at each projection angle with the respective last updated ray-sum. The corresponding correction is distributed over the pixels in the image and weighted by the distance to the related X-ray path. This updating procedure in the ART algorithm is very time-consuming, leading to the implementation of an analytical reconstruction procedure, the filtered back-projection (FBP). ART in its original design requires more time per iteration than a complete reconstruction by FBP with comparable accuracy in image quality.[14] However, IRTs are more flexible in incorporating, for example, complex reconstruction geometries and noise statistics modulation, and are less sensitive to the number of projections used in the reconstruction.[15] Due to the difference in reconstruction speed, FBP has been the gold standard in reconstruction techniques in clinical CT scanners since the mid-1970s. About three decades later, the difference in computational time between some IRTs and FBP had become insignificant due to the increased power of reconstruction computers. In addition, due to the many advantages of the iterative approach in reconstruction mentioned above, the major CT manufacturers then started to

reintroduce IRTs as a complement to FBP. These IRTs use an FBP image from which the iteration procedure was started, some manufacturers gave the operator the option of choosing the numbers of iterations for the reconstruction and other manufacturers construct a fusion image consisting of the iterated image and the FBP image.

The quantum noise is the main factor limiting the minimisation of the absorbed dose for a CT examination reconstructed using FBP, as the noise may become too high and obscure important anatomical structures or pathology. Hence, the IRTs were primarily reintroduced to reduce quantum noise. The reintroduced iterative reconstruction algorithms used a model of noise based on Bayesian statistics in the updating procedure of the image.[16] Each pixel in the CT image consists of a CT number describing the capacity of the imaged material to attenuate X-rays (see section 1.2 'Image quality'). One part of this model is the regularisation step, in which pixels with CT numbers far from its neighbours' CT numbers are called to be updated. Some of the random noise in the image will be reduced in this step since the random noise is unrelated to its neighbours. A regularisation step is typically nonlinear as it adapts to preserve sharp edges in the image.[15] This framework also offers the possibility of weighting down noisy projections in the reconstruction procedure to maximise the contribution of projections with good quantum statistics.[15] In addition to reduction of noise, some beam-hardening artefacts are also reduced, as has been shown in clinical studies.[17,18] Further development of the algorithms includes modelling of, for example, the geometry of the focal spot, the imaged object, and the detector element to be represented by areas or volumes instead of points. These later models will contribute to improvements in spatial resolution of the CT images.[15] One disadvantage of the noise reduction part of an IRT is, as mentioned above, the fact that it is often nonlinear, and the smoothing of a nonlinear algorithm can alter the appearance of the image to look unfamiliar to the radiologist and other concerned medical professions.

FBP is a linear reconstruction technique, and image appearance can be modified using convolution kernels. The image content can be divided into the imaged object and the noise. According to the theory of linear systems, the image content can be described using spatial frequencies. Further, the imaged object to a larger extent than the noise is composed by lower frequencies. Hence, by application of a low-pass kernel, noise will be reduced more than the imaged object. However, sharp edges also consist of high frequencies and will consequently also be suppressed by such a kernel. Hence, a dose reduction using a low-pass kernel will then be limited to the required spatial resolution of the specific CT examination. Another advantage of using linear reconstruction techniques is the possibility of generalising measurements of image quality to be

valid for any imaged part of the patient body. In contrast, a nonlinear regularisation will introduce an image quality that cannot be generalised, as the regularisation is dependent on the contrast of the imaged structures in the patient or the noise level. Other nonlinear algorithms that can be implemented in an iterative reconstruction, may also generate artificial structures.[19] Such structures could be mistaken for or obscure pathology and lead to a misdiagnosis. Generation of artificial structures is most common in metal artefact reduction (MAR) and has been studied by many, both clinically and through phantom studies.[20–22] In CT imaging for diagnostics and also in the planning of radiotherapy treatment,[23] the reduction of metal artefacts often outweighs the generation of other types of artefacts induced by the MAR algorithms.[24,25] Although the risk of artificial structure generation is higher due to the mechanisms in some MAR algorithms,[26] there is still a possibility that nonlinear noise reduction may induce structures mimicking pathology.

In summary, the effects of nonlinear noise reduction algorithms may increase image quality and support the radiologist in the diagnostic process. Further, the image quality may be altered such that radiologists' experience of how pathology is depicted in CT imaging is no longer applicable. Thus, the present thesis investigates some of the effects of nonlinear noise reduction algorithms on clinical image quality and how the effects can be analysed.

1.2 Image quality

A CT system depicts the linear attenuation coefficient of an acquired object, which describes the capacity of the depicted material to reduce radiation. Since the attenuation is dependent on the energy of the X-ray photons, the coefficient value is presented in relation to water and referred to as CT number. The definition of CT number is expressed as follows:

$$\text{CT number} = 1000 \cdot \frac{\mu_{material} - \mu_{water}}{\mu_{water}},$$

where $\mu_{material}$ and μ_{water} are the linear attenuation coefficients of the estimated material and water, respectively. Hounsfield unit (HU) is the unit of CT number. The CT system is calibrated, for each X-ray spectrum used, to assign water and air the CT numbers 0 HU and -1000 HU, respectively. Spatial resolution and noise in an image affect the reproduction of the CT number and are two fundamental quantities that are often used to describe image quality. These quantities are described below to provide a short introduction to what a nonlinear noise reduction algorithm can affect.

1.2.1 Spatial resolution

Spatial resolution refers to the ability to resolve two measured values from each other; in image physics this is equivalent to the smallest spacing between two imaged objects. In CT imaging, the maximum spatial resolution is often specified as line pairs per centimetre at full width at half maximum, i.e. how many reconstructed lines of equal width of line and spacing can be fitted in one centimetre before the lines are not able to be separated. An ideal imaging system would be able to fit an infinite number of lines, i.e. the system would be able to reproduce an edge without any blur. However, in a CT imaging system there are various limitations that will reduce its ability to reproduce sharp edges. For example, let us consider an X-ray film with no screen imaging system, where all the variations of the attenuation of the examined object must be detected to be able to fully reproduce the object in an image. Even though the 'detector elements' of the film are at the size of micrometres, the film will still not have reproduced a fully clear image, as the object will scatter the X-ray photons to the surrounding 'elements'. Further, the area of the X-ray focal spot will generate a geometrical distribution error of the X-ray photons, known as penumbra shading. In CT imaging, the geometrical error will be even larger, as the detector elements are larger than the grains in photographic film and the projections are only approximately acquired continuously around the object, due to technical limitations such as data storing and after-glow in the detector (limiting a reasonable acquisition time). All these phenomena will increase the uncertainty in the separation of the linear attenuation coefficients in the object. If the system is linear, the generalised spread caused by the CT system can be estimated by the point spread function (PSF), which is often acquired by imaging a thin highly attenuating object. A common practice is to calculate the discrete Fourier transform of the PSF to estimate the modulation transfer function (MTF). Modulation refers to the amplitude of a sinusoidal signal relative to the average of the sinusoidal signal. Further, the MTF is defined as the ratio of the modulation of the signal in an image to the modulation before the imaging of the signal at each spatial frequency, i.e. how much of a specific spatial frequency has been transferred to the image (for further information on the subject, see section 1.4.2 'Objective evaluation of resolution and distortion in nonlinear systems' and 3.3.1 'Theory of assessing resolution').

1.2.2 Noise

Noise can be interpreted as statistical variations in measurements, and in a digital image the variations generated by an X-ray system can be divided into quantum

noise and electronic noise. In an X-ray imaging system composed of a source and a detector array, the measurements consist of letting a number of photons pass through an object to estimate the attenuation of the object. The probability of the X-ray photons interacting with the object medium (not reaching the detector) will for example depend on the thickness and electron density of the object and the energy of the photons. The number of photons reaching the detector in a period of time follows a Poisson distribution. Hence, the array of detector elements will demonstrate signal variations (quantum noise) dependent on this distribution. The measurements obtained by a detector may further be disturbed by electronic noise, due to current variations in the hardware components of the CT system. These variations are often small compared to the quantum noise for an energy integrating detector. However, the effect of electronic noise becomes more substantial as the number of detections is decreased.[27] Both the quantum and electronic noise will be represented as random variations of the CT number in the image, and one study has proposed that the electronic noise may be compound-modelled as Gaussian.[28]

The standard deviation of the pixel values in a region of interest (ROI) is often used as a measure of noise magnitude. However, the appearance of the image noise will depend on the spatial frequencies represented in the noise. The analysis of noise magnitude in a digital system can then be extended to measure the power of the noise at individual frequencies using the concept of noise power spectrum (NPS).[29] Analysis of NPS in CT systems can indicate the texture of the noise, and the NPS may vary between manufacturers and model of CT scanner.[30] Thus, compared to standard deviation, the use of NPS improves image quality assessments.[31]

In a CT system, the noise is transferred from the projections to the reconstructed image. The transferred noise will be correlated depending on the reconstruction technique used and the geometry in which the projections are acquired. In the case of geometrical dependence, the noise magnitude in a reconstructed image will follow a radial relationship, as patients can often be approximated as cylindrical objects. Hence, the X-ray beam will face a thicker object in the middle of the beam as it is rotating around the patient. Consequently, the statistical variations will be higher in the middle detectors, and the magnitude of the noise will be higher in the centre of the reconstructed image. This geometrical phenomenon is almost always true in clinical situations. Hence, clinical CT systems are always equipped with physical filters of low density, known as bowtie filters, to shape the photon flux to be lower at the ends and higher in the middle of the fan-beam, such that the noise magnitude in the detector array, and consequently also in the reconstructed image, will be more homogeneous. Consequently, the use of bowtie filters also requires the scanned object to be placed in the isocentre of the CT gantry. Otherwise, the noise will be higher and

may even be more heterogeneous than without a bowtie filter. However, in a clinical situation, the magnitude of the noise is most often sufficiently homogeneous to be measured using standard deviation or NPS. Although the noise is approximately homogeneous, the complexity of analysing image quality of CT systems increases when reconstruction parameters are applied. For example, filter kernels (see 1.3.1 'Filter kernels'), iterative reconstruction and noise reduction algorithms (see 1.3.2 'Iterative reconstruction and nonlinear noise reduction') can be used to adapt image quality to the clinical task and are unique to manufacturers, which may complicate comparisons between CT systems. Methods have been developed to consider these parameters.[31–35] However, the complexity of nonlinear noise reduction algorithms still needs further investigation, and some of the complexities are within the scope of the present thesis.

1.3 Noise reduction techniques

The ability to detect and locate pathology, such as lesions, may be affected by the contrast between the lesion and the surrounding anatomy, the size of the lesion, and the noise in the CT image.[36] The strategies for reducing the influence of noise, i.e. decreasing the random variations of the CT number, can be represented by reconstruction algorithms and postprocessing techniques. A noise reduction reconstruction algorithm used in a CT system is applied in the reconstruction domain and can be categorised as filter kernels or iterative reconstruction algorithms. The iterative algorithms can use models of the quantum statistics or the geometry of the CT system to reduce noise. In contrast, a postprocessing technique is applied directly to the reconstructed image. The algorithms in all categories can be either linear or nonlinear. The kernels and iterative noise reduction algorithms provided in the CT scanner have manufacturer-specific product names, even though the mechanism may be similar.

1.3.1 Filter kernels

Filter kernels are part of the FBP algorithm, which is based on the theory of back-projection. A back-projection reconstruction technique can roughly be described as evenly spreading the acquired projections back along the paths of the X-rays. Intuitively, this technique will distribute attenuation values at positions that have not attenuated the X-ray photons in the acquisition. Consequently, attenuation values of objects may also be underestimated, as these projection values are evenly distributed at other positions. Thus, the result of a back-projection reconstruction

is a blurred image of the acquired object. To compensate for the blurring, the acquired projections can be filtered in the frequency domain by multiplication of a ramp filter. The amplitude of the linear ramp increases with frequency and will hence work as a high-pass filter, which reduces the low frequency components and emphasises the high frequency components.[37] A back-projection algorithm using this type of filter defines the FBP algorithm. The filtering in the FBP algorithm can be described in the spatial domain as deconvolving the blur generated by the back-projection algorithm. The filter ramp can be combined with a second filter which then changes the weighting of the spatial frequencies. The combination is called convolution kernel and is often constructed to weight down the highest frequencies. A suppression of these frequencies will increase the contrast-to-noise ratio (CNR) in a reconstructed image, as such weighting will reduce the noise more than the contrast. However, as sharp edges of structures in the patient also consist of high frequencies the weighting must be adapted dependently. Thus, the CT manufacturers have often incorporated several types of convolution kernels suited to the different examination types. The ability to differentiate between white and grey matter (brain tissue) in cerebral examinations is mainly dependent on the contrast difference rather than the delineation of structure borders. Such examinations can benefit from a highly smoothing convolution kernel that reduces the random noise as noise can obscure the contrast differences more than the delineation of the structure borders. The convolution kernel used in paediatric cerebral examinations part of the investigation in Paper I is highly smoothing and was used at the clinic due to the diagnostic task. The dependence of type of convolution kernel in combination with an iterative noise reduction was one of the aims in the investigation in Paper II.

Image processing using a mean or a median filter works as a smoothing convolution kernel and may be applied directly to the image or the projection data to reduce noise. These filters operate in the spatial domain and will function more or less as a low-pass frequency filter in the frequency domain, depending on the shape of the kernel. The median filter preserves the signal values and does not fabricate new ones, as the mean filter does, which can make the median filter better in edge preserving. However, the mechanism of a mean filter is linear, as the output of the filter is directly proportional to the change in the input.[38] In contrast, the median mechanism is nonlinear and may cause signal distortion (see 1.4.2 ‘Objective evaluation of resolution and distortion in nonlinear systems’). The nonlinear behaviour of the median filter is investigated in Papers III and IV.

1.3.2 Iterative reconstruction and nonlinear noise reduction

An IRT in CT imaging is based on comparisons between the forward projections of an estimate of the object and the real acquired projection data. The estimated projection data is acquired by simulating a CT system which is virtually forward projecting the reconstructed image as if it was the object. The comparison between the real and estimated projection data is used to compute a correction term based on the various built-in models in the reconstruction algorithm. The first iteration is finished when the correction term has adjusted the reconstructed image. The process can be stopped after a fixed number of iterations, when the correction term is small enough or an image criterion is reached. For the two latter stopping conditions, the closer the estimate of the object is to the real object, the fewer iterations are required for the process to converge to a stable solution. Hence, an CT image reconstructed using FBP is frequently used as an initial estimate.[39] The forward projections of the FBP image will not be identical to the acquired projections, due to the quantum variations in the detected signal. The iteration process of the FBP image may change the noise appearance. Hence, some manufacturers fuse the iterative reconstructed image with an FBP image to preserve some of the noise appearance that radiologists are familiar with. The adaptive statistical iterative reconstruction (ASiR™, GE Healthcare, Milwaukee, WI, USA) can be fused in steps of 10% up to 100% (0% ASiR is the same as an FBP reconstruction and these terms are used interchangeably throughout the thesis; 100% ASiR implies only the ASiR reconstruction) and is the noise reduction algorithm investigated in Papers I and II. The ASiR algorithm is based on the iterative coordinate descent algorithm and uses the statistical properties in the intensity measurements from the CT scanner to reduce noise.[16,40]

The iterative approach of reconstructing CT images has the advantage of updating the pixel values in an image based on the properties of the CT system. These properties can be divided into optical and physical parameters, and noise statistics. The FBP algorithm models the optics using only one X-ray pathway to represent the beam of X-rays from source through the object to the detector. In contrast, an IRT is able, for example, to model the area of the X-ray focal spot, the object volume, and the detector array to consist of many subregions. The number of possible pathways increases with each subregion, which enables more precise estimation of the linear attenuation coefficient in the volume element (voxel). The result is increased resolution and a reduction in systematic errors such as streaking artefacts. However, this procedure may depend on the location of the objects in the image of the patient and will thus not fulfil the requirements of a linear system. Further, the computation time also increases as the number of equations in the system follows the number of pathways. Consequently, the

strategy of using subregions is often omitted or approximated by a gaussian distribution to speed up the reconstruction time.[16]

The X-ray beam used in CT imaging is polychromatic, which is not accounted for in a reconstruction using FBP. An iterative reconstruction approach can model the interaction of a polychromatic beam in the focal spot, the object, and the detector to reduce artefacts due to beam hardening.[26,41] Other physical properties that could be incorporated in the model may be to not allow negative values of the linear attenuation coefficients, as this would imply that X-ray photons are created rather than attenuated. Even if exclusion of the non-negativity constraint would violate fundamental physics, the benefits of the constraint in diagnostic CT are questioned.[42] Further, the distortion properties of the constraint is investigated in Paper III.

Models of noise statistics can be applied in the projection domain (pre-processing) or in the image domain (post-processing) and can be independent of the reconstruction algorithm.[43–46] Such models are based on maximising the posterior probability using the Bayesian framework, i.e. what is the most probable attenuation coefficients based on the measured projection data. Hence, these models can assign a confidence level to the measured values which are being updated, based on the variation in relation to their surrounding values. Further, the attenuation differences of human tissues are relatively small in comparison to the variations in the noise. Hence, the noise could be distinguished from the linear attenuation coefficient of human tissue as the estimated values of the coefficient should fall in a reasonable range. Thus, a common strategy to reduce noise in a CT image of a patient is to minimise the total variation (see section 3.4.4 'Nonlinear noise reduction algorithms used in the simulations' for a short description of the algorithm) as this type of minimisation will penalise noise more than the structures of the patient.[47,48] The total variation algorithm is nonlinear, and the distortion properties of this filtration are further analysed in Paper IV. Another strategy for the pre-processing algorithms is to weight the projections depending on the noise level of the measured values, such that projections with high noise are given lower confidence and will contribute less to the correction term.[49] The same logic of the updating process can be assigned to post-processing, where unrealistic CT numbers are penalised and modified more than a CT number that does not diverge much from the neighbouring pixels. The process of assigning confidence to the measured projection values is nonlinear as it typically adapts to preserve the spatial resolution of the imaged object while reducing the noise.

The correction term obtained from the noise model can be back-projected using FBP or used to update the pixels in the image by an iterative strategy. The strategy differs between the iterative algorithms, as described above; the ART algorithm updates the image ray by ray, in contrast to the simultaneous iterative

reconstruction technique (SIRT), which updates all the pixels in the image concurrently for each iteration. For example, the correction for one projection angle can be performed for all pixels before another projection angle can correct the image or the contribution of all projections angles can be used to calculate the correction.[50] The iterative process aims to minimise the residual between the forward projection data and the obtained projection data from the CT examination. The minimum is usually a non-zero positive value as the projections are inconsistent due to noise, and the minimum may be found by different strategies. The conjugate gradient least-square (CGLS) algorithm uses the concept of conjugate direction to find the minimum.[51] Without a nonlinear noise model, such an iterative process is linear. The distortion caused by a SIRT algorithm and a CGLS algorithm in combination with a median filter and a total variation reduction algorithm, respectively, is analysed in Paper IV.

1.4 Evaluation of image quality

Image quality can be evaluated using human observers and mathematical measures in the image. These methods can be divided into two groups: subjective evaluation and objective evaluation, where mathematical measurement is always objective. However, a human observer evaluation measures image criteria based on psychophysical determinations and can only be considered as objective when a ground truth is given to compare with in the analysis. Without the ground truth, the evaluation measures the observer's subjective opinion of the image quality. The choice of evaluation type may be dependent on the study task, as an observation made by a radiologist is more likely to correlate to a clinical task than a number derived from measurements of the physical image.[52] On the other hand, mathematical measurements may determine differences between imaging systems more conveniently than human observer studies, as long as the image quality is measured correctly. A combination of the two evaluation methods should be considered if the diagnostic value of the whole imaging system is to be assessed.[53]

1.4.1 Human observer evaluation

A study using human observers where the ground truth is known may be considered as more clinically relevant than a study analysing the image quality based on the opinion of observers. However, an observer study of known pathology can be difficult to perform, as it requires images of patients with and

without the specific pathology.[53] Further, the collection of a sufficiently large sample size of images and the process of constructing the true answers of the pathology may be very time-consuming. In addition, the study preparations cannot be too long, as the study may become irrelevant when the study is finished. An alternative is to simulate pathology into the images of a patient with negative findings to increase the sample size.[54–56] However, another alternative is to set up an observer study of anatomical structures and let the observers grade how well these structures are reproduced, known as visual grading (VG). The theory of VG is based on the fact that radiologists detect pathology by comparing the findings with their experience of healthy structures, i.e. if the anatomy can be reproduced well, then so can the pathology. Although VG studies have been subject to criticism, as a determination of beauty rather than diagnostic value, the method is widely used and has been indicated to be as clinically relevant as a study of pathology.[57]

VG may be used to grade image quality relatively by comparing the structures between two or more images. The image quality can also be assessed on an absolute verbal rating scale, where one image at a time is graded using ordered adjectives of visibility. The data from an absolute VG study is ordinal and must be treated according to rank-invariant properties in the statistical analysis, i.e. the result of the verbal rating is only dependent on the order and not the labels.[58,59] Quite a few statistical methods have been developed that are appropriate to these types of studies.[60–62] Further, the data may also be paired in cases where two different methods are compared by viewing the exact same reproduced region in the patient. The human observer studies in the present work (Papers I and II) are VG studies with paired ordinal data.

1.4.2 Objective evaluation of resolution and distortion in nonlinear systems

The image quality of CT images may be estimated using mathematical measures of the image such as the spatial resolution and noise. The spatial resolution is often described in terms of the MTF, which estimates the ability of the imaging system to reproduce isolated spatial frequencies of the object. The NPS is used to describe the frequency content of the noise in the image. These image quality metrics can be generalised for any input in a system that fulfils the requirements of linearity, i.e. additivity and homogeneity.[63] Additivity states that the sum of two inputs transferred through a system should be equal to the sum of the two inputs after they have been separately transferred through the same system. This can be mathematically written as:

$$H\{f_1(x,y) + f_2(x,y)\} = H\{f_1(x,y)\} + H\{f_2(x,y)\},$$

where H is the system working on the input functions $f_1(x,y)$ and $f_2(x,y)$. The homogeneity condition states that the result of a scalar factor working on an input before it has been transferred through a system is equal to the result of the scalar working on the output of the same system, provided the same input. Mathematically, this is written as:

$$H\{\alpha f(x,y)\} = \alpha H\{f(x,y)\},$$

where α is a scalar. Although real systems are never strictly linear, an approximation of the linear-system characteristics may be justified. The introduction of iterative noise reduction algorithms in CT imaging has complicated this justification as the often-applied regularisation term is highly nonlinear. The consequences of the nonlinearity in CT imaging systems have been shown to be resolution-dependent on the noise level and the contrast level, both in phantom studies[34,64–67] and visually in clinical studies.[68] Further, the noise has been shown to be non-stationary and dependent on the imaged object.[69,70] Furthermore, the object and the noise in the image have been shown to be distorted to other frequencies[71] and to have generated new types of artefacts, such as plastic-like appearance (especially in noise reduction) or object generation (especially in MAR). Studies have proposed task-specific metrics to overcome the issue of noise and contrast dependence.[72] Based on the theory of MTF, the task transfer function (TTF) was developed to estimate the transfer of a signal at a specified contrast and noise level relevant to the task. A similar approach has been proposed to calculate a task-specific NPS.[34] The NPS can be shifted by a nonlinear algorithm and generate a noise texture different to noise reconstructed using FBP, which might make the radiologist uncertain of the diagnosis.[73] As a consequence of these findings, the developers of the noise reduction algorithms started to adapt the algorithms to better match the reconstruction of FBP.[74–76]

In nonlinear systems, even if the NPS is task-specific it may not indicate changes in the noise texture due to a dependence on the content of the background, as the NPS is calculated in a homogeneous background. However, studies have proposed the noise to be segmented based on the noise magnitude to calculate the noise characteristics using the autocorrelation.[69,77] Further, the unavoidable distortion effects are often ignored in these modifications of metrics, based on the linear-system theory, as the distortion effect is assumed to be embedded in the metric. However, the distortion effects embedded in the TTF may not correspond to the distortion of the analysed task. A study by Wells and Dobbins[71] has

separated the distortion effects from the signal modulation using a methodology to obtain the proposed principle frequency response (PFR), which is equal to the MTF for a linear system, and the distortion power spectrum (DPS), which corresponds to the distortion power of individual frequencies. The methodology was developed and tested on conventional radiography systems, and the scope of Paper III was to implement the methodology for CT systems. Further, the distortion effects may also vary depending on the composition of the object. Hence, an analysis of individual frequencies may not fully grasp the distortion effects in patient images. Thus, Paper IV proposes a methodology to visualise the distortion of objects and noise caused by nonlinear noise reduction algorithms.

Many diagnostic tasks can be interpreted as detection procedures, i.e. whether the radiologist can detect a pathology or not. Since human observer studies can be rather time-consuming, this has led to the development of a method that can mathematically describe the detection of, for example, a lesion in a CT image of a patient. This mathematical model of an observer is called model observer and can either be ideal or filtered in one way or another to match the diagnostic task, e.g. often mimic observation by a human eye. The model observer concept is based on the separation of the probability distribution of a signal (e.g. a lesion) present or not present in a background (anatomy plus noise). In a linear imaging system, the signal task is filtered using the image quality properties of MTF and NPS and often also by the visual response of a human observer. The result is an index that describes the probability that the signal is detected, the detectability index (d').[35,78] The use of mathematical models can be extended to include modelling of all steps in an observer study, including the acquisition of the images, the examined patient, and the diagnostic evaluation of the detected pathology. This concept is known as virtual clinical trials.[79,80] The TTF and task-specific NPS have been implemented in the model observer formalism to account for some of the nonlinear effects of noise reduction algorithms and have recently also been determined in clinical images.[81,82] The effect of distortion on the image quality has not yet been properly investigated, and some methods to analyse these effects will be explored in the present thesis.

2. Aims

The overall aim of the work in the present thesis was to investigate the effects of nonlinear noise reduction algorithms in computed tomography imaging. The aim was split into four separate studies, the first two studies investigating the effect subjectively and the last two objectively. The aims of the separate studies were:

1. To investigate the effect of a nonlinear noise reduction algorithm on the diagnostic image quality in paediatric cerebral CT imaging (Paper I).

2. To investigate the dependence of diagnostic image quality of a nonlinear noise reduction algorithm on type of convolution kernel in paediatric abdominal CT imaging (Paper II).

3. To implement objective metrics for resolution and distortion effects in nonlinear CT imaging (Paper III).

4. To develop methods for visualising the distortion of object and noise caused by nonlinear noise reduction algorithms in CT imaging (Paper IV).

3. Materials and Methods

Papers I and II investigate the effect of a nonlinear noise reduction algorithm on image quality in clinical images using human observer evaluation, while Paper III and IV focus on describing the changes in image quality through measurements in the image using simulations of the CT systems and the scanned objects.

3.1 The clinical computed tomography system

All major CT manufacturers provide clinical systems equipped with nonlinear noise reduction algorithms. In the present thesis, the effect of one nonlinear noise reduction algorithm on the clinical image quality was investigated. All methods described below were intended to be applicable to any CT system independent of the manufacturer. The objective method of analysing resolution and distortion implemented in CT in Paper III requires access to the projection data, which can only be provided by the manufacturer. In Paper IV, the objective methods developed for analysing the nonlinear distortion of object and noise also required access to the projection data. However, an approximation of the method for analysing the nonlinear distortion of object was proposed to perform the analysis on image data only. These mathematical estimations of the distortion effects were mainly investigated using basic nonlinear algorithms to understand more easily what the methods are capable of analysing.

3.1.1 Acquisition parameters

The same clinical CT system was used in the two observer studies (Papers I and II). The system was a 64-slice Discovery CT 750HD™ scanner (GE Healthcare, Milwaukee, WI, USA) located at the Paediatric Radiology Department of Queen Silvia Children's Hospital, Gothenburg, Sweden.

The acquisition of the projections could be performed in two modes on the present system. One mode acquired images by scanning the patient using a step and shot technique (axial mode), where each rotation was acquired at fixed positions of the patient, i.e., the patient table was stationary during the collection of projection data. The other mode acquired the projections as the patient table was moving through the gantry and was called helical mode in the present system. One advantage of the axial mode and the reason for using it in the acquisition of

cerebral examinations (Paper I), was the possibility of tilting the gantry, such that the eyes of the patient were not irradiated directly by the X-ray beam and absorbed dose to the lens was avoided. The helical mode was used for abdominal examinations (Paper II), as it could cover a larger length of the patient faster and more conveniently, due to continuous movement of the patient table. One disadvantage of the helical mode, in comparison to the axial mode, was that a larger length of the patient must be irradiated to be able to reconstruct images of the same volume in the patient (overranging; Figure 2).

The detector array of modern CT system consists of several rows along the patient, and the system used in Paper I and II was able to simultaneously acquire 64 image slices with an image thickness of 0.625 mm on one rotation using the axial mode. Hence, the collimation width of the X-ray beam for such acquisition must be just over 40 mm to also compensate for the effect of the penumbra on both sides. The signals from the detector rows can be combined to acquire thicker slices, consequently the number of images will then be reduced. Reconstruction of thick slices may be more beneficial than batching thicker slices from thinner

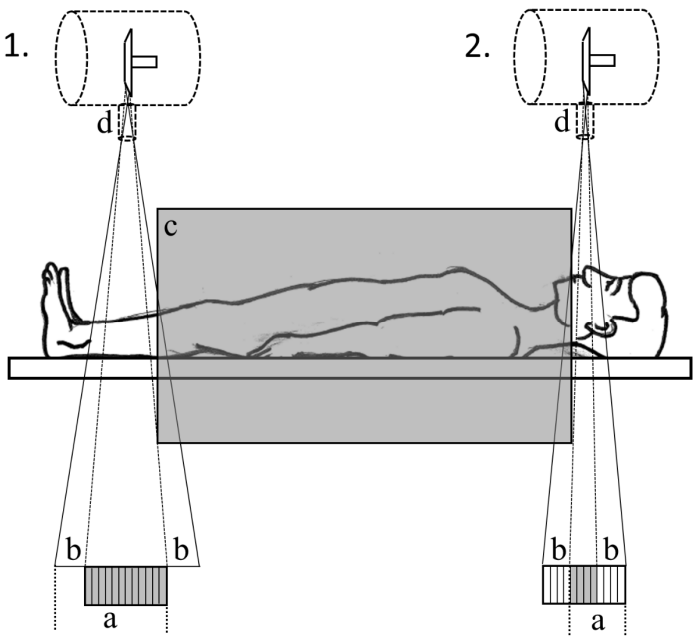

Figure 2. Illustration of the overranging (a) and the overbeaming (penumbra; b) required to obtain images of the whole reconstruction volume (c) and full radiation flux to the detectors respectively. The difference in overranging and overbeaming between two different collimation widths (d) is shown, where the first setup used the whole detector array (1.) and the second used the detector array partially (2.).

reconstructed slices. However, the latter approach may be more convenient in a clinical workflow. The overranging distance is often minimised by active collimation, as the whole detector array is not used for the slice at the end of the reconstruction volume. The collimation width is then reduced by shifting one of the collimators actively at the start and stop position of the reconstruction volume.[83] Further, the collimation could be adjusted to optimise between overranging and overbeaming (penumbra; Figure 2), but also scattered radiation, and speed of the examination. Overbeaming describes the increased beam width along the patient, due to geometrical effects such as the size of the focal spot. The overbeaming area does not contain full beam flux and is not used for reconstruction of images and will only contribute to more absorbed dose to the patient. Hence, large collimation is preferable for whole-body examinations as the number of overbeaming areas will be lower. However, using the helical mode, a smaller collimation may be more dose-efficient for shorter scanning distance, as the overbeaming may contribute less to the total absorbed dose than the overranging could have contributed to with large collimation. Further, small collimation would generate less scattered radiation to the active detectors, while large collimation could cover a longer part of the patient faster. A collimation of 20 mm was used for all cerebral examinations and for the youngest children of the abdominal examinations, while a collimation of 40 mm was used for the older children.

In helical mode, the ratio between the patient table increment to the total collimation width defines the pitch. Hence, a pitch smaller than one indicates the patient being irradiated with an overlap, a pitch of one is an edge-to-edge scanning acquisition, and a pitch larger than one irradiates the patient with a gap. The pitch of the abdominal scans was close to one, 0.984.

The fastest rotation time of the system was 0.4 s and was used for the abdominal examinations to decrease the scanning time and possible artefacts, due to respiratory motions. The risk of motion-artefacts in cerebral examinations was smaller, which allowed a slower rotation time of 0.6 s. A longer rotation time also allowed a larger number of projections per rotation and consequently often a better spatial resolution. However, in examinations of children, a fast scanning-time may be crucial for a good examination, as unpredicted motion may occur more frequently compared to adults. Hence, the rotation time could not be chosen to be too long.

The standard tube voltage for adult examinations of both the head and the body has been 120 kV. However, it could be more dose-efficient to scan small patients using a lower tube voltage, especially children. Hence, the youngest patients at the clinic were scanned using 100 kV. The relationship between image quality from

different tube potentials and absorbed dose has been studied more thoroughly by other authors.[84,85]

Tube current modulation is provided in various configuration by the manufacturers. However, the main purposes of these utilities are to vary the tube current depending on the attenuation properties along the patient (z-modulation) and around the patient (x/y-modulation), as a patient tends to be more ellipsoidal than cylindrical. A modulation utility searches to keep the standard deviation in an image constant throughout the examination by correlating an index to the acceptable quantum noise. A more thorough description of the tube current modulation can be found elsewhere.[86,87] The configuration of the present system modulated the cerebral examinations using z-modulation and the abdominal examinations using x-, y-, and z-modulation. The index of which the modulations were controlled was named noise index (NI) on the CT scanner used, where a low value of NI indicated a low standard deviation. The NI was set lower for younger children, as the contrast in anatomy increases with age. The NI was also dependent on the slice thickness of the reconstructed image, as thicker slices have lower standard deviation than thinner slices. However, the NI was independent of filter kernel as the standard deviation of reference was calculated in an image of water reconstructed using FBP and the filter kernel called 'Standard'. The cerebral and abdomen examinations were acquired with an NI related to an image slice thickness of 5 mm and 0.625 mm respectively. The reason for scanning using thin slices of 0.625 mm was to be able to batch image series in the coronal and sagittal planes of the patient, while the cerebral examinations were only viewed in the axial plane at that time and did not have to be reconstructed in thin slices.

It was important to consider the shape of the bowtie filter regarding the size of the examined body part. There were two shapes of the bowtie filter designed to even out the detector signal and thereby also the dose gradient in the patient. Each of the shapes was limited to a circular maximum reconstruction region, which was called scan field-of-view (SFOV) on the present CT system. The SFOV of the smaller bowtie filter was 32 cm, while the SFOV of the larger filter was 50 cm in diameter. In general, the larger SFOV was used for adult (or children of the same size) body examinations and the smaller SFOV was used for head examinations and body examinations of the smallest children. Head examinations must have a reconstruction correction to decrease artefacts due to the skull bone. Hence, the choice of a small SFOV also included a choice between head and body examination.

In a CT system, the weighted computed tomography dose index ($CTDI_w$) estimates the absorbed dose for one rotation divided by the width of the beam collimation.[88] Further, the $CTDI_w$ is determined using the axial scanning technique on a cylindrical polymethyl methacrylate (PMMA) phantom. A

phantom of diameter 32 cm is used for estimations of the absorbed dose for a body CT examination and a phantom of 16 cm is used for a head examination. Furthermore, the smaller phantom is sometimes used to estimate the absorbed dose for CT examinations of children. Absorbed dose for a CT examination performed using the helical scanning technique is determined by dividing the $CTDI_w$ with the pitch to form the volume averaged CTDI ($CTDI_{vol}$). The standard of reporting these dose metrics is in unit of milliGray (mGy). In theory the $CTDI_{vol}$ is independent of the scanning length and the total dose for a CT examination can be estimated by the multiplication of $CTDI_{vol}$ by the scan length, which forms the dose length product (DLP). Therefore, this metric is in unit of milliGray centimetre (mGycm). Table 1 in Paper I and Table 1 in Paper II list the estimated $CTDI_{vol}$ for each age group. It should be noted that the $CTDI_{vol}$ is an index estimated to PMMA and should not be used to estimate dose to individual patients. Recently, size-specific dose estimate (SSDE) has been proposed to be a dose estimate specific to the size and density of irradiated volume of the patient.[89–91]

3.1.2 Raw data collection

Clinically preformed paediatric CT examinations of the cerebrum (Paper I) and abdomen (Paper II) were the subject of interest, as these were the most frequent and most dose-heavy CT examinations, respectively. Further, the cerebral and abdominal examinations were performed without and with intravenous contrast medium, respectively. The acquired examinations were stored locally on the CT system in a raw data format (projection data). Further, anonymised raw data of the subjects were retrospectively collected and stored on local hard-drive disks as the CT system could not store more than approximately one month of patient examinations. The criteria for inclusion were examinations using standard examination parameters and with no pathological findings or motion artefacts that could disturb the assessment of the anatomical structures. The number of patients was also limited due to time, as the scanning protocols had to be kept the same and without updates of the CT systems. A collection time of approximately one year was considered to be reasonable, as by then the number of included patients had reached 20 (Table 1).

3.1.3 Reconstruction of raw data

The only available noise reduction algorithm on the CT system at the time of the studies was ASiR (see section ‘1.3.2 Iterative reconstructions and nonlinear noise

reduction'). The clinic had implemented a 30% level of ASiR for cerebral and abdominal scans following the recommendation of the manufacturer. The applied ASiR level was accompanied by an increased NI to use the gained noise reduction, as an action to save on absorbed dose. The same raw data of each patient was retrospectively reconstructed at the percentage levels of ASiR used in the studies (Table 1). The batching of the image series was carefully performed to generate images at the same location in the abdomen for all the series of different levels of ASiR. Only axial images were reconstructed and used in the investigations as the image evaluation software ViewDEX (Viewer for Digital Evaluation of X-ray images) used in the investigation had not yet implemented an option of simultaneously view multiple stacks.[92–95] The cerebral and abdominal examinations were reconstructed into image stacks of 5 mm thick slices. A stack of the whole cerebral examination was used to evaluate the image quality of the anatomical structures, while a smaller region (4 cm in length) was used for the evaluation of the abdominal examinations. The location of the region was carefully specified to contain the relevant anatomical structures of the investigation for each patient. The reason for using a smaller region was to reduce the time for observer evaluation. The number of images in each stack used in the observer studies was approximately the same for the younger age groups. Hence, the paediatric heads were quite small, and the image slices of the head were reconstructed edge-to-edge, compared to the abdominal images, which were reconstructed with 50% overlap.

Table 1. Study information of the patient groups assessed in Paper I and Paper II. The table includes the assessed ASiR levels and convolution kernels for the patient material, where bold marks the reference (original) parameters.

	Cerebral study (Paper I)		Abdominal study (Paper II)		
Group	A	B	A	B	C
Age range	5-18 y	0-5 y	2-15 y		
Assessed ASiR levels	0%, 20%, **30%**,40%, 50%, 60%, 100%	0%, **30%**, 40%, 50%, 60%, 70%, 80%, 100%	**30%**, 50%, 70%, 90%, 100%		
Convolution kernel	**Soft**	**Soft**	**Soft**, Standard, Detail		
No. of patients (in intra observer study)	20 (3)	20 (3)	35 (4)		
Viewed cases	161	184	585		
No. of observers	3	3	4		

The convolution kernel used at the clinic for the present examination types was a smoothing type of kernel called 'Soft' on the CT system. The 'Soft' kernel was used as a noise reduction tool, which also smoothed out edges. The reason for investigating the effect of the convolution kernel in Paper II was the results from the cerebral examination in Paper I. It showed the delineation of one of the structures representing sharp edges ('cerebral fluid space around the brain', Table 2) to degrade as the level of ASiR increased to 100%. Such degradation might be due to the combination of the 'Soft' kernel and the level of ASiR, since the smoothing of the edges could have become more prominent when the noise was further reduced by the ASiR algorithm. Hence, the observer study of the abdominal examinations investigated the effect of combining a more edge-enhancing filter kernel with ASiR. Consequently, the number of cases for the observers to view in Paper II increased threefold, as three filter kernels ('Soft', 'Standard' and 'Detail') were investigated.

Table 2. The assessed questions of anatomical structures and diagnostic image quality with corresponding rating scale used in Papers I and II. The anatomical structures are highlighted by bold text.

	Cerebral study (Paper I)	Abdominal study (Paper II)
	Questions about the anatomical structures	
Q1	How well can you differentiate **white and grey matter**?	How well is the **aorta** delineated?
Q2	How well are the **basal ganglia** delineated?	How well are the **hepatic veins** delineated?
Q3	How well is the **ventricular system** delineated?	How well is the **liver delineated against the abdominal wall**?
Q4	How well is the **cerebrospinal fluid space around the mesencephalon** delineated?	How well is the **extra-hepatic part of the portal vein** delineated?
Q5	How well is the **cerebrospinal fluid space around the brain** delineated?	How well is the **pancreas** delineated?
Q6	How well are the **vessels in the pentagon cistern** delineated?	How well is the **diaphragmatic crus** delineated?
	Question about the diagnostic image quality	
Q7	For what diagnostic situation is this image quality sufficient?	Grade the diagnostic usefulness of this image quality for a standard abdominal examination
	Rating scale for Q1-6	
A.	Clearly	A. Clearly
B.	Acceptably	B. Acceptably
C.	Poorly	C. Poorly
D.	Not at all	D. Not at all
		E. Not applicable
	Rating scale for Q7	
E.	For high-resolution diagnostics	
F.	For standard diagnostics	F. Excellent
G.	For low-resolution diagnostics	G. Sufficient
H.	Not diagnostically useful	H. Insufficient
		I. No diagnostic use

3.2 Observer evaluation of image quality in nonlinear systems

3.2.1 Visual grading

The number of CT examinations of paediatric patients without pathological findings was low (Table 1). However, the number of examinations with a specific pathology was even lower. Hence, it was suitable to use visual grading for the evaluation of image quality of the paediatric CT scans at the clinic (Paper I and Paper II). The visual grading approach was absolute, as the cases were evaluated separately using a scale of verbal rating (Table 2). A case was defined as one patient's reconstructed image series using one specific set of reconstruction parameters. Each case was rated using six questions related to the anatomical structures and one question about the diagnostic image quality (Table 2). The categories of the rating scale described how well the anatomical structures were reproduced (Table 2). The categories used for Question 7 in Paper I described for what diagnostic situation the image quality was sufficient and in Paper II the categories described the diagnostic usefulness of the image quality for a standard abdominal examination (Table 2). The ratings were paired data, as the same raw data of each patient was reconstructed with different reconstruction parameters and evaluated against the reference parameters (Table 1). All cases in the studies were presented to each observer in a unique random order, without annotations of patient information or scanning parameters to reduce possible biases in the observer ratings in the assessments.

Since the observer studies used quite few patients and few observers, it was important to consider the intra-observer variability to identify possible changes in observer ratings, i.e. an intra-observer study. The intra-observer study identified one observer to have changed his/her way of using the rating scale during the assessment of the first patient group (Group A, Table 1), who was asked to reassess all the images in this substudy. The data from the reassessment was then used in the analysis. The intra-observer study consisted of three to four patients related to each group of assessed patients, where the image stacks were duplicated and reconstructed at all studied levels of ASiR (Table 1). The intra-observer study was integrated in the studies and was not known to the observers. As each of the intra-observer cases was assessed twice, the first assessed case was used in the observer evaluation.

The observer evaluation was assessed on the same computer using a monochrome medical LCD monitor (EIZO RadiForce G33; Nanao Corporation,

Ishikawa, Japan). In the image evaluation software ViewDEX,[92–95] the image stack of the cases was presented together with a digital questionnaire bound to the viewed case. The observers were allowed to use zoom, pan, and change the window width and window level of the images and to stop the session at any time to take breaks, when assessing the anatomical structures. However, the observers did not have the option to revisit a case after assessment of it was finished. The observers were able to calibrate their rating scale by visiting a training session before each trial of assessment or after breaks. The cases in the training session were not included in the study as they did not fulfil the inclusion criteria.

The questions used in the evaluation were implanted with small changes from previous studies by Ledenius et al.[96,97] The choice of structures was based on including image quality markers of high- and low-contrast diagnostics. Both clinical studies (Papers I and II) also included a question of the diagnostic value, which was used to represent the overall image quality.

Variations in the assessments between observers with different experience might exist. Hence, for the evaluation to be valid for a large group of radiologists, the radiologists participating as observers in the studies were chosen to represent different specialities (radiology, paediatric radiology and paediatric neuroradiology) and time in the field of radiology (range: radiology resident in radiology to about 25 years of practice).

3.2.2 Statistical analysis

The observer evaluation resulted in paired ordinal data, which had systematic and random variability. The nonparametric method of Svensson was used to separate these variabilities and to analyse the probability of a change in the observer ratings between the assessed image qualities.[60,98,99] For each observer, the rating of each question for the clinical reconstruction settings used (30% ASiR had been implemented before the studies) was the reference and paired with each rating of the same question for the tested reconstruction parameters. Hence, in Paper I, the level of 30% ASiR was paired with each other tested level of ASiR. Further, in Paper II, the filter kernel of ‘Soft’ together with the level of 30% ASiR were the reconstruction parameters of reference and paired with each other combination of filter kernel and level of ASiR. In practice, the frequency distributions of the paired assessments were placed in cross-classification tables to calculate percentage of agreement (PA), relative position (RP), relative concentration (RC) and relative rank variance (RV). A closer description of these metrics has been made by others.[60,100] In summary, the PA was the percentage of cases with equal rating, i.e. no difference between the reconstruction parameters.

The RP and the RC described the probability of a systematic difference for the frequency distributions, in contrast to the RV, which described the random difference. The RP and RC ranged between values of -1 and +1. Negative values of RP indicated the proposed reconstruction parameters to be systematically rated with lower categories in comparison to the reference, i.e. a lower category in the present studies describes better reproduction of the image. Further, a positive RC indicated the distribution of the ratings for the reference to be more centrally located on the rating scale, i.e. some cases were better reproduced, while other cases were worse reproduced using the proposed reconstruction parameters. A value of RC well separated from zero could indicate that something had disturbed the assessment. The RV ranged from 0 to +1 and a value diverging from zero indicated variability isolated from the systematic variability of the ratings.

3.3 Objective assessment of resolution and distortion in nonlinear systems

The scope of the second part of the present thesis was to develop an objective method to assess the degradation in image quality observed in Papers I and II. The possible distortion caused by the nonlinear noise reduction algorithm was proposed to be one of the explanations and was intended to be assessed in Paper III and IV. To the author's knowledge, the signal response of nonlinear CT systems had never been isolated from the distortion. Hence, a methodology developed for conventional radiology was implemented in CT systems in Paper III, where the response of individual frequencies was isolated from the distortion. In Paper IV, the implemented methodology (Paper III) inspired development of a more accessible method that could be applied to existing CT systems.

In comparison to the theory of linear systems, there is no obvious method to objectively evaluate image quality of a nonlinear system. Methods that have been proposed to take the nonlinear behaviour into consideration have adapted the traditional metrics of resolution and noise to be task-specific. However, such adaption may not be sufficient to evaluate the image quality of an image reconstructed using nonlinear noise reduction, as it has been shown that nonlinear systems may transform signal power of a spatial frequency to other frequencies (Figure 3). Hence, the distortion effect must be explored to ensure that the image quality induced by nonlinear noise reduction algorithms can be approximated to be analysed using the methods based on the theory of linear systems.

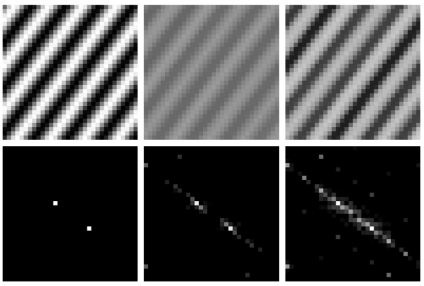

Figure 3. Impact of nonlinear noise reduction on a 2D sinusoid, showing signal power to be transferred to other frequencies. The sinusoid is presented in the image domain (top row) and in the Fourier domain (bottom row). The original sinusoid (left) has been noise reduced in the projection domain by a median filter (middle) and by a total variation filter (right) and reconstructed using a FBP algorithm. In rows, the image domain and the Fourier domain plots are equally windowed and levelled. The intensity in the Fourier domain plots is at log scale.

3.3.1 Theory of assessing resolution

The theory of linear systems implies that for a linear system any signal can be described as a composition of sinusoidal waves. Hence, the resolution of the system can be defined as the ability to reproduce sinusoids of all spatial frequencies. Consider an imaging system that will reproduce an infinitely narrow signal, for example a delta function. The delta function must implicitly be described using sinusoidal waves of all spatial frequencies without any change in the modulation, as a delta function is represented by a straight horizontal line in the frequency domain, i.e. an ideal system with perfect resolution must transfer an infinite number of sinusoidal waves with equal amplitude as the input, at all spatial frequencies to give an output of the delta function without any spread. Unfortunately, no existing imaging system is ideal and, consequently, the response in the delta function is called the PSF. This means that for a non-ideal imaging system the ratio between the output and input amplitudes of transferred frequencies will be less than one. Thus, the Fourier transform of the PSF will give

the relative amplitude at all spatial frequencies, i.e. the system MTF, and describe how well a system can reproduce individual spatial frequencies. In practice, the narrow signal is approximated using a thin wolfram wire or a sharp edge of a phantom. The latter method is used for the task-specific metric TTF.[64]

3.3.2 Objective assessment of resolution in nonlinear systems

The method of estimating resolution using a delta function may not be valid in a nonlinear system, as signal power may be transferred to other spatial frequencies (distort) and corrupt the estimation of the PSF (point spread function). Further, the resolution of a system can equivalently be estimated by presenting individual sinusoids to the system and analysing the proportion of the transferred amplitudes.[29,101] Hence, by isolating the response of individual spatial frequencies the resolution can be estimated isolated from the distorted frequencies using the PFR, which is equivalent to the MTF for a nonlinear system.[71] The PFR is estimated using discrete 2-dimensional sinusoidal patterns. In the frequency domain, a continuous 2-dimensional sinusoid is represented by two mirrored complex values (dots) specific to the spatial frequency. Hence, the pixel positions of the frequency response are easy to locate for the sinusoids (Figure 4a). However, the patterns must be limited to the reconstruction area and such limitation will convolve the dots with a sinc function (Figure 4b). Fortunately, the discretisation of the sinusoid will lead to sampling of the frequency domain at positions where the sinc function is zero if the sinusoid is a period of the reconstruction field of view (FOV; Figure 4c). Thus, the change in magnitude of the spatial frequencies is estimated by the ratio between the absolute value of the pixel positions before and after the sinusoid has been transferred through (reconstructed by) the system (Figure 4d). Consequently, the PFR values range between 0 and 1 if no edge enhancement has been applied to the reconstruction. The maximum number of spatial frequencies in an estimation of the resolution using PFR is dependent on the size of the reconstructed FOV. The spatial frequencies may be sampled more sparsely to accommodate the power of the computer processor and storage capacity, as long as the frequencies are a period of the FOV size. The array size of the PFR was chosen to 32×32, as this size was used by Wells and Dobbins. Each sinusoid was sampled at different phase shifts to average the estimation of the distortion effect and resolution, 30 phase shifts were used in Paper III as some phase shift led to null values. Further, a background containing noise was added to the sinusoids to investigate the dependence of the resolution of a nonlinear system on noise level. Background noise was simulated

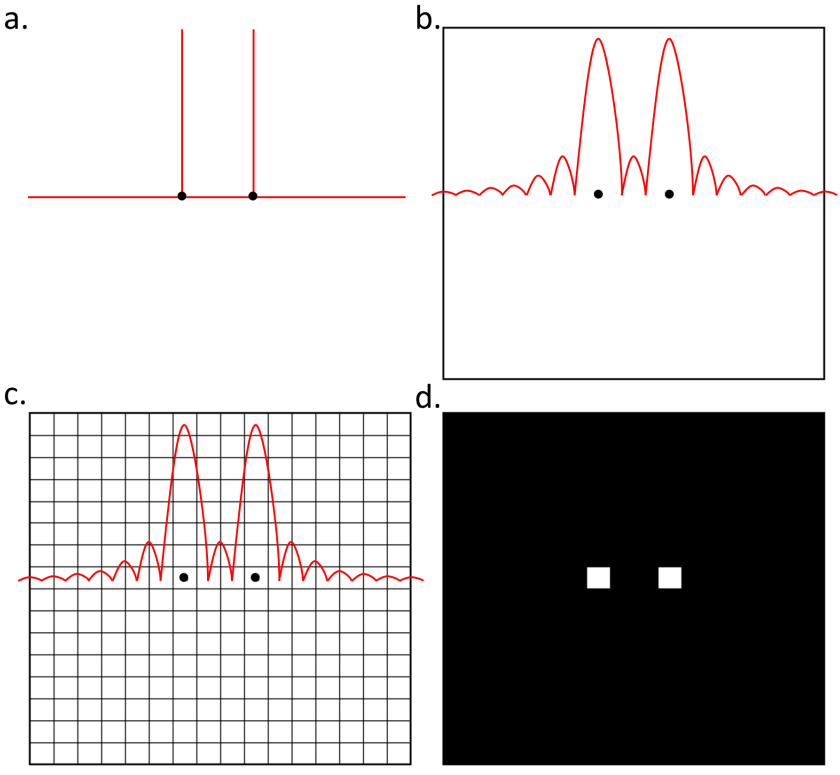

Figure 4. Schematic illustrations of a 2-dimensional sinusoid in the frequency domain, the red lines represent the absolute value of the 1-dimentional profile over the dots representing the sinusoid. The dots for a continuous 2-dimensional sinusoid are represented by delta functions (a), for a limited reconstruction area the dots are convolved with a sinc function (b), the discretisation of a sinusoid with period of the field-of-view is sampled when the sinc function is zero (c), and the change in magnitude of the sinusoid may be measured at these discrete pixel positions (black corresponds to zero signal and white to the magnitude; d).

only once for each sinusoid. However, the estimation at each spatial frequency was calculated using the same number of noise samples as the phase shifts, since the noise was resampled for each phase shift. The sampled sinusoid was repeated over the array of the reconstructed FOV. In Paper III, the number of repeated sinusoids was 256, as the size of the array was 512 × 512.

The nonlinear algorithms added to the system were a median filter, representing a nonlinear noise reduction algorithm, and a non-negative constraint, representing a common nonlinear mechanism in iterative reconstruction (Paper III). The simulation workflow of the PFR was as follows (Figure 5):

1. Generation of 2-dimensional sinusoidal patterns with a number of periods of the size of the reconstructed FOV and equal amounts of phase shifts. The number of sinusoids used in Paper III was 32 × 32 spatial frequencies and 30 phase shifts, i.e., 1,024 evenly spaced spatial frequencies each at 30 phase shifts, a total number of 30,720 reconstructions for one noise level.

2. Forward projection of the sinusoids to projection data.

3. Application of a Poisson-distributed noise related to the projection data. The process is repeated for the number of background samples used in the estimation. In Paper III, one sample of noise was used, however the period of the sinusoid with the largest wavelength was repeated 256 times in that noise sample. The noise was also resampled at each phase shift and the sinusoid was consequently then analysed in at least 7,680 unique noise backgrounds.

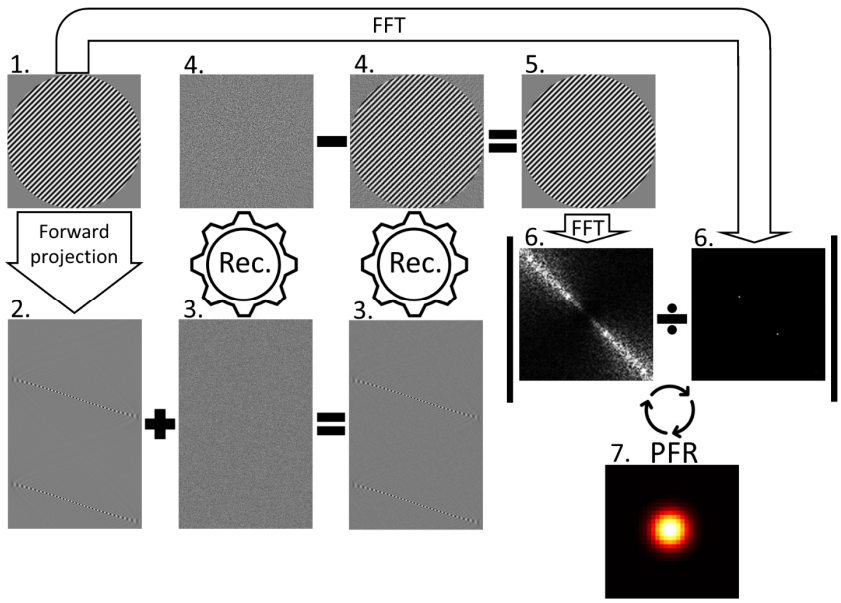

Figure 5. Illustration of the workflow for the calculation of the 'principle frequency response' (PFR). The squared objects at (1.), (4.), and (5.) are presented in the image domain and the rectangular objects at (2.) and (3.) represent the projection data of (1.) and (4.). The squared objects at (6.) represent the fast Fourier transform (FFT) of the images at (1.) and (5.), and (7.) represents the PFR of the analysed nonlinear algorithm. The cogwheels indicate reconstruction, and the arrows are marked with forward projection or FFT, vertical lines indicate absolute value, and the circle arrows indicate that the calculation is repeated for each analysed frequency, phase and background. The numbers (1.-7.) are related to the workflow described in the text.

4. Reconstruction of both the noisy projection data and the noise data separately, using the same nonlinear algorithm.

5. Subtraction of the reconstructed noise from the reconstructed noisy sinusoid to generate a sinusoid consisting of the original spatial frequency and the distorted frequencies caused by the nonlinear algorithm.

6. Comparison in the frequency domain between the absolute values of the pixel positions for the sinusoid obtained in 5. and the original sinusoid.

7. Averaging of the ratio obtained in 6. over the number of phase shifts and the number of background samples for each spatial frequency to obtain the array of PFR.

3.3.3 Theory of assessing distortion

Distortion is defined here as the transfer of power from one spatial frequency to another (Figure 3). According to this definition, aliasing is a type of distortion. Aliasing can induce what are known as moiré patterns in the image and occurs when the object has been sampled too sparsely to only reproduce that object. Consider a continuous sine wave, which has been sampled at discrete positions too sparse to accurately reproduce the spatial frequency of the sine wave. These sample positions can fit both the continuous sine wave and at least one other sine wave of a lower frequency. Hence, an image of the sample points will appear as these spatial frequencies. Thus, signal power of the high frequency could be said to have been transferred to a lower frequency. Such under-sampling may induce distortion artefacts in images of all digital systems, both linear and nonlinear.

Distortion artefacts in images are complex to evaluate, and many different methods have been proposed to assess the effect of the artefacts and correlate them to the perception of the human eye. Although the origin of many of these methods is from image compression, some methods are used in medical imaging evaluation.[102–104] These objective methods assess changes of the physical image using numerical values based on various variation metrics. The metrics may be related to the mean squared error and the peak signal-to-noise ratio. However, in some cases such metrics do not correlate with human observations.[105] Hence, adaptations to the human visual system have then been made to the metrics by introducing schemes weighing the differences based on structure information or statistical information, e.g. structural similarity index,[106] visual information fidelity[107] and most apparent distortion.[108] The most apparent distortion scheme combined two strategies to change between dependent on the type of distortion in

the image. One of the strategies is used for images containing just-visible distortions and the second one is for more obvious distortions. However, the mentioned methods do not distinguish between if the distortion is caused by a linear or nonlinear system.

3.3.4 Objective assessment of distortion in nonlinear systems

The proposed methods in Paper III and IV are developed to assess distortion in nonlinear systems.

3.3.4.1 Distortion power spectrum, distortion index, ΣDI & $\overline{DI}$

The previous mentioned method developed by Wells and Dobbins (see, 3.3.2 'Objective assessment of resolution in nonlinear systems') that isolates the PFR from distortion also estimates the DPS. A nonlinear system may transfer signal power dependent on the spatial frequencies in the signal. However, the distortion caused when imaging a delta function (containing all spatial frequencies) may not correspond to the waveform distortion of sinusoids at individual spatial frequencies. Hence, the DPS summarises the power of the distortion at an array corresponding to the sampled spatial frequencies of the PFR array. The DPS array represents the power of transferred distortion to all sampled frequency positions other than the spatial frequency of the investigated sinusoid, i.e. DPS does not represent the summarised power distorted to the spatial frequency of the corresponding sinusoid. The metrics PFR and DPS can be combined to characterise the ratio of the distortion to the transferred sinusoidal signal by a distortion index (DI).[71] The DI is inspired by the total harmonic distortion, a metric used for analysing 1-dimensional nonlinear waveform distortion in the engineering community.[109–111]

The DPS was estimated using sinusoidal patterns, and the first five steps in the simulation process of PFR described in section 3.3.2 'Objective assessment of resolution in nonlinear systems' were equal to those for DPS. However, to obtain the DPS steps 6. and 7. were changed, as follows (Figure 6):

6. A notch filter ignoring the pixel positions of the sinusoid was applied in the frequency domain when the absolute distortion values was summed up and averaged over the number of background samples used in the estimation.

7. The output from 6. was squared and multiplied by the dimensions of the reconstructed FOV array (i.e. number of pixels and the widths of a pixel) to convert the output units to reflect the signal power.

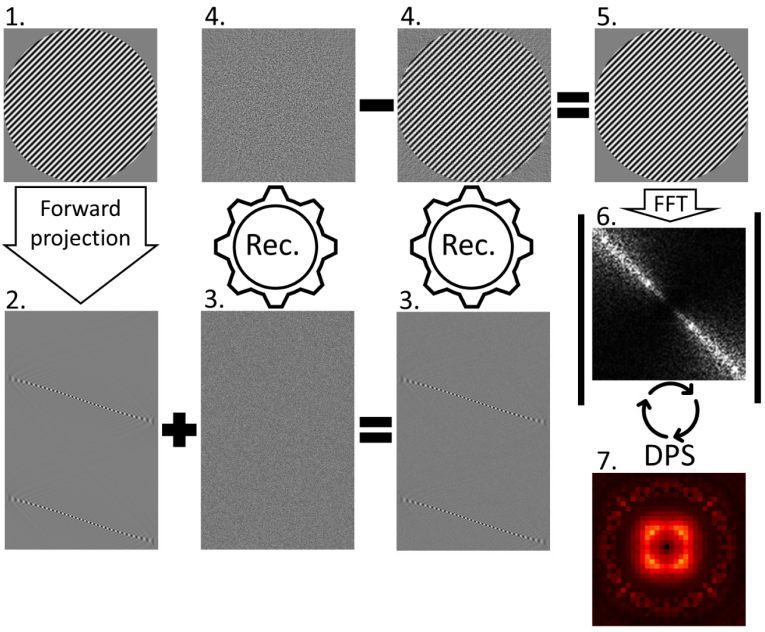

Figure 6. Illustration of the workflow for the calculation of the distortion power spectrum (DPS). The squared objects at (1.), (4.), and (5.) are presented in the image domain and the rectangular objects at (2.) and (3.) represent the projection data of (1.) and (4.). The squared object at (6.) represents the fast Fourier transform (FFT) of the image at (5.), and (7.) represents the DPS of the analysed nonlinear algorithm. The cogwheels indicate reconstruction, and the arrows are marked with forward projection or FFT, vertical lines indicate absolute value, and the circle arrows indicate that the calculation is repeated for each analysed frequency, phase and background. The numbers are related to the workflow described in the text.

The DI was calculated as an array equivalent to the arrays of PFR and DPS, and two figures of merit, sum of DI (ΣDI) and mean of DI ($\overline{\text{DI}}$) were determined. The DI array was calculated to reflect the fraction of the output signal power at each sampled spatial frequency.[71] The ΣDI was the sum of all the distortion power divided by the total output signal power, i.e. the distortion fraction of the system at the specified noise level. The mean distortion fraction could also be estimated using $\overline{\text{DI}}$ which was the sum of all the distortion fractions at each sampled spatial frequency divided by the number of sampled spatial frequencies (Paper III). The $\overline{\text{DI}}$ reflected the appearance of the DI array and was less sensitive to changes in the total output signal power. For example, a system with low resolution could be

described by ΣDI to have low distortion, even if the distortion fraction at individual spatial frequencies was 100 percent. The same system could be described by $\overline{DI}$ to have high distortion, even if the distortion at the individual spatial frequencies was barely visible due to the low resolution of the system. Hence, the choice of figure of merit was dependent on the question, i.e. was the distortion fraction of interest dependent on (ΣDI) or independent of ($\overline{DI}$) resolution of the system. However, a comparison between systems is easiest when the systems have equal power of the total output signal.

3.3.4.2 Nonlinear distortion of objects and noise, NLD_{object} & NLD_{noise}

If the imaging system is nonlinear, the sum of distortion at individual sinusoids (ΣDI or $\overline{DI}$) may not be equal to the distortion of an image composed by the same sinusoids, i.e. the distortion may be dependent on the composition of the imaged object. Further, a nonlinear noise reduction algorithm may not only distort the object but also the noise. The appearance of the distortion may also be of interest, as the composition of the distorted spatial frequencies can mimic or obscure the pathology. Hence, Paper IV intended to develop a method to visualise the distortion in nonlinear CT systems.

The method was divided into two types of image visualising distortion of the object and noise induced by a nonlinear noise reduction algorithm. The method was inspired by the technique of isolating distortion from frequency response described by Wells and Dobbins[71] and later implemented in CT systems by the present author (Paper III). The method presented in Paper IV was adapted to isolate the nonlinear difference of a system by comparing the two sides in the superposition principle. The residual between the two sides describes to what extent the system was nonlinear, and for a residual close to zero the system was assumed to be linear. In the calculation of the first type of image, the nonlinear distortion of objects (NLD_{object}), one of the sides represented several noisy projection data that were first averaged and then reconstructed into an approximately noise-free image. The other side represented the same noisy projection data that were first reconstructed and then averaged into an approximately noise-free image (Figure 7). The residual between these sides was the NLD_{object} and was calculated using the following workflow:

1. Projection data of an object were acquired repeatedly over the same volume at the noise level of interest and duplicated into two sets. The number of acquisitions was dependent on the noise level to generate an NLD_{object} with reasonable low variations to visualise the systematic distortion.

2. For the first set of noisy projection data, the object was reconstructed in the presence of noise by the following steps:

    a. The noisy projection data were reconstructed separately to noisy images of the object.

    b. The noisy images were averaged to an approximately noise-free image, where the averaged image represents the object and the systematic effect of the reconstruction algorithm in the presence of noise.

3. For the second set of noisy projection data, the object was reconstructed in the absence of noise by the following steps:

    a. The noisy projection data were averaged to approximately noise-free projection data.

    b. The projection data obtained in 3a. was reconstructed to an approximately noise-free image, where the image represents the object and the systematic effect of the reconstruction algorithm in the absence of noise.

4. The averaged image obtained in 3b. was subtracted from the image reconstructed in 2b. to obtain the NLD_{object}, which represents the distortion of the object dependent on the noise level and number of repeated acquisitions for a nonlinear system.

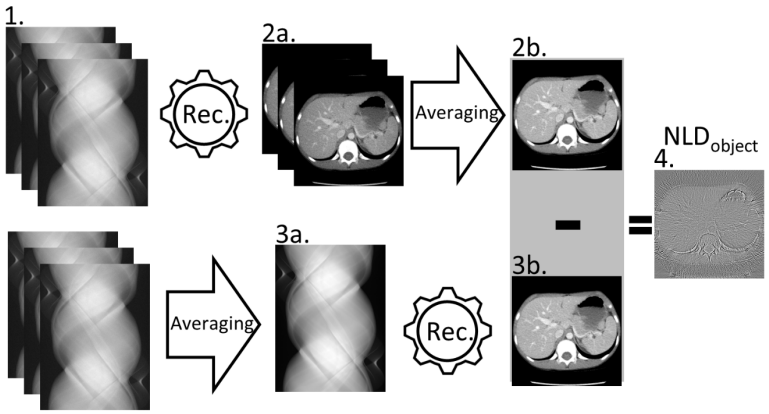

Figure 7. Illustration of the workflow for the calculation of the nonlinear distortion of objects (NLD_{object}). The cogwheels and arrows indicate reconstruction and averaging, respectively. The numbers are related to the workflow described in the text.

In the second type of image, the nonlinear distortion of noise (NLD_{noise}), the noise was isolated and reconstructed with and without the object present. Hence, one of the sides represented the isolation of noise after reconstruction and the other side the isolation of noise before reconstruction. The isolation of noise was done after and before the reconstruction by subtracting the average of the noisy images from each noisy image and the average of the noisy projection data from each projection data respectively (Figure 8). The residual between these sides was the NLD_{noise} and was calculated using the following workflow:

1. Projection data of an object was acquired repeatedly over the same volume at the noise level of interest and duplicated into to two sets. The number of acquisitions was dependent on the noise level to generate an NLD_{noise} with reasonable separation of the object.

2. For the first set of noisy projection data, the noise was isolated after reconstruction by the following steps:

    a. The noisy projection data were reconstructed separately to noisy images of the object.

    b. The noisy images were averaged to an approximately noise-free image.

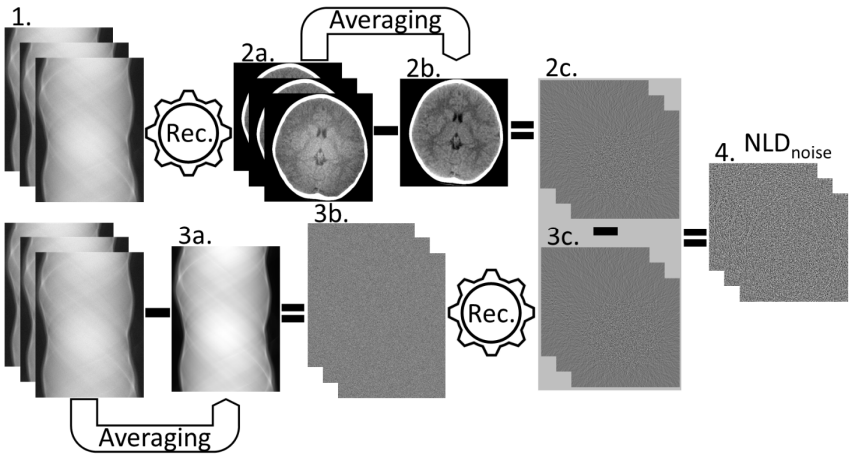

Figure 8. Illustration of the workflow for the calculation of the nonlinear distortion of noise (NLD_{noise}). The cogwheels and arrows indicate reconstruction and averaging respectively. The numbers are related to the workflow described in the text.

c. The image obtained in 2b. was subtracted from each noisy image obtained in 2a. to isolate the images of noise only, where the images represent the effect of the reconstruction algorithm on noise reconstructed in the presence of the object.

3. For the second set of noisy projection data, the noise was isolated before reconstruction by the following steps:

    a. The noisy projection data were averaged to approximately noise-free projection data.

    b. The projection data obtained in 3a. were subtracted from each noisy projection data to isolate the projection data of noise only.

    c. The projection data of noise obtained in 3b. were reconstructed separately to images of noise only, where the images represent the effect of the reconstruction algorithm on noise reconstructed in the absence of the object.

4. The noise images obtained in 3c. were subtracted from the respective noise images obtained in 2c. to obtain the NLD_{noise} series, which represent the distortion of the noise dependent on the noise level and number of repeated acquisitions for a nonlinear system.

The NLD_{object} and NLD_{noise} visually described the distorted spatial frequencies of the object and noise respectively. The NLD_{object} could detect the noise dependence of the nonlinear noise reduction algorithm, as the systematic distortion difference between reconstructing noisy projection data and approximately noise-free projection data was calculated. Further, the NLD_{noise} could detect how the noise was distorted by the reconstruction depending on the object, as the object was reconstructed with and without the object.

The NLD_{object} and NLD_{noise} had to be calculated through manipulations in the projection data. However, an approximation of NLD_{object} (NLD'_{object}) could be estimated by replacing the approximately noise-free image by a separately acquired image with low noise. Hence, estimation of the NLD'_{object} was possible on an existing CT system without access to manipulation of the projection data. The noise was not static between acquisitions and cannot be replaced in a second acquisition.

3.4 Simulation of a computed tomography system

An existing CT system at a clinic has limited access to the projection data, i.e. the data are locked to saving, loading, and retro reconstruction using the built-in algorithms. Hence, most of the manipulation of projection data used in the methods described in section 3.3 'Objective assessment of resolution and distortion in nonlinear systems' cannot be performed on a CT system at a clinic without permission from the manufacturer. Thus, simulation of a computed tomography system was suited to use when testing these methods for analysing resolution and distortion effects of nonlinear noise reduction algorithms.

3.4.1 Configuration of the simulated geometry

The purpose of the investigations was to assess resolution and distortion induced by a nonlinear CT system. The required geometrical elements for the simulation of such a CT system were a source and detector array rotating around (projection geometry) an object (volume geometry) and a reconstruction algorithm based on these geometries. The geometries of the CT systems in Papers III and IV were simulated using the open source Compute Unified Device Architecture (CUDA)-integrated toolbox ASTRA©[112–114] for MATLAB™, due to the easily handled code and the variety of integrated reconstruction algorithms. The projection data from the simulation were generated through forward projection of the object based on the projection and volume geometries.

In the simulation of the projection geometry, the detector array was limited by the toolbox to a flat configuration, where the width of the detector array was defined as the number of detectors multiplied by the distance between the centres of two adjacent detector elements. The fact that a large array of detectors would generate long reconstruction times was taken into consideration, when the detector width of around 1 mm defined at the iso-centre and the number of detectors was set to 737 and 1,474 in Papers III and IV respectively. The flat configuration mimicked what is known as a cone-beam CT system more than a conventional CT system. However, the outcomes of the studies were to be used as examples of how the distortion could be assessed. Hence, an exact geometrical configuration was not critical to validate the proposed methods.

The source was configured as a fan-beam, where the projection geometry simulated diverging X-rays using the width of the detector array, the distance between the source and the isocentre, and the isocentre and the detector array. The distances used in the simulation originated from a rather old clinical CT system. The projection positions were defined by the degree and range of the angles. The

number of projection angles was kept at 1,152 and was evenly spaced around the object (geometry of 2π).

The simulation of the volume geometry was limited by the toolbox to a centrally positioned array when the graphics processing unit (GPU) was used. There was a possibility that the sharp squared objects used in Paper III might interfere with the analysis of the DPS. Hence, a circular mask was used to reduce long vertical and horizontal edges of the object. Further, a typical clinical CT image consists of 512 × 512 pixels, and the geometry of the reconstructed volume of one image slice was specified to 768 × 768 pixels in the simulations. Thus, a ROI of the same size as a clinical image (512 × 512 pixels) could be used to analyse the frequency content well within the borders of the object. Another reason to ignore the outer region of the reconstructed area was that possible differences in the distortion effects due to the geometrical difference between an arc or flat detector array could be reduced.

3.4.2 Simulation of noise

The dependence of a nonlinear algorithm on noise was assessed at a range of noise levels. In Paper III, the analysis of the distortion effects was based on sinusoidal objects with an amplitude of unity and a mean of zero. Hence, it was logical and convenient to define the greatest variation from zero of the sinusoids as the contrast and use a contrast-to-noise ratio (CNR) to define the level of noise. There exist many methods of measuring CNR, and the differences are mainly in the estimation of the noise.[115] The standard deviation in Paper III was estimated in the noise image reconstructed without the object, which was connected to one of the lowest frequencies evaluated. In Paper IV, a typical abdominal CT image was used to illustrate the concept of the method. In this image, a CNR was defined as the difference between the CT numbers of muscle and liver tissue (avoiding the hepatic veins filled with contrast medium) divided by the standard deviation of the CT number in the muscle tissue (here defined as the background). The CNR was estimated using sufficiently large ROIs to generate stable standard deviation values. The standard deviation was estimated in the muscle ROI as this has been recommended by others to be used as background.[115] The CNRs of the sinusoid and the typical abdominal CT image were both defined in images reconstructed using FBP.

In Paper III, the sinusoidal objects for which the noise was simulated were scaled to represent maps of linear attenuation coefficients, which was calculated to range from the coefficient of dry air (near sea level) to that of liquid water. The linear attenuation coefficients listed in the NIST database were used in the

studies.[116] The forward projection data had to be transformed from linear attenuation to detector signal by the Beer-Lambert law before a quantum noise could be added. The added noise was calculated from a Poisson distribution where the expectation values followed the attenuation of the object. In Paper IV, noise was simulated as if the intensity of the CT image ranged from dry air (near sea level) to that of cortical bone.

3.4.3 Reconstruction algorithms used in the simulations

The analytical reconstruction algorithm, FBP, used the Ram-Lak and Hamming filters. The Ram-Lak filter is a ramp filter that only compensates for the blur of the back-projection and, unlike the Hamming filter, does not reduce noise by weighting down image components of the highest frequencies. The Ram-Lak filter was used in Paper III to show the distortion of all frequencies without any noise reduction. In Paper IV, the smoothing by the Hamming filter was compared to the noise reduction of the median and total variation filter.

The methodology used in Paper III was implemented from conventional radiography and has never been tested in CT. Hence, it might be important to investigate basic and understandable reconstruction algorithms or nonlinear mechanisms. The iterative reconstruction algorithm SIRT and the non-negative constraint were investigated, as they were well-known and quite easy to understand. An initial test of the integrated algorithms of the toolbox indicated that the CGLS algorithm behaves differently to the SIRT algorithms. Hence, both these algorithms were chosen to test the developed methodology of assessing distortion in Paper IV.

3.4.4 Nonlinear noise reduction algorithms used in the simulations

The median filter and the total variation filter were chosen, due to their simplicity and their frequent use in medical imaging,[117] to demonstrate the methods for analysing the distortion induced by the nonlinear noise reduction algorithms. The most basic adaptation of the filters was used to explore the utility of the metrics derived from the methods. The nonlinear noise reduction algorithms were only applied to the projection data before the reconstruction of all algorithms and not internally implemented in the iterative reconstruction algorithms to keep the algorithm complexity low. The median filter used in Papers III and IV returned the median value at a kernel size of 3×3. The values outside the boundaries of the

projection data array were extended symmetrically, i.e., mirror-reflecting the array across the array borders in an attempt to reduce border distortion.

Total variation denoising is based on minimising the L^1 norms of derivatives, which represent the total magnitude of the variations in an image.[47] A noisy image has clearly higher total variation than a noise-free image (Figure 9). Hence, updated estimates of the image regularised by minimisation of the total variation will have less noise. Further, these estimates will be independent of the image, as the total variation of a smooth image is the same as the total variation of a sharp image, i.e., sharp edges will not be updated to become smoother due to the minimisation of the total variation (Figure 9). Even if sharp edges may be preserved, regularisation by total variation encourages the image to be less complex. Hence, loss in complex structures may occur when the regularisation is too high. The total variation de-noising is nonlinear and more complex to compute compared to de-noising based on least square errors.

The total variation algorithm used in Paper IV had two regularisation parameters, lambda (λ), which controlled the amount of denoising, and number of iterations, which indicated the number of repeated corrections of the denoised image. The parameters were set to match the reduction of the standard deviation caused by the median filter in an image reconstructed using FBP.

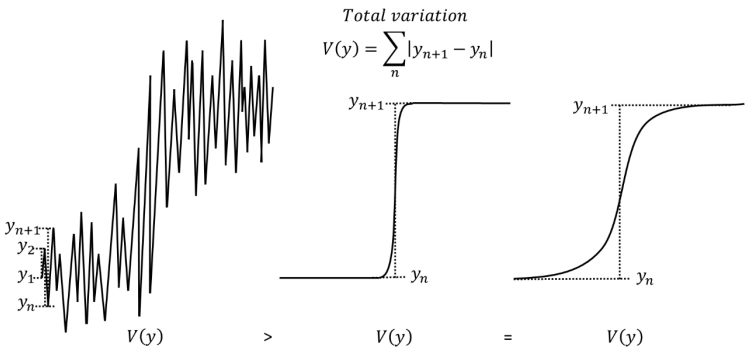

Figure 9. Schematic illustration of the total variation of a noisy edge (left), a sharp edge (middle), and a smoothed edge (right). The total variation is obviously greater for the noisy edge and equal between the sharp and smoothed edges, meaning that an updating procedure minimising the total variation will not favour a smooth edge over a sharp edge.

4. Results and Discussions

4.1 Subjective effect of nonlinear noise reduction

4.1.1 Paediatric cerebral computed tomography (Paper I)

In Paper I several anatomical structures were investigated to find the specific structures affected by the nonlinear noise reduction. The structure that stood out from the rest was 'the cerebrospinal fluid space around the brain' (Cerebral study (Paper I), Question 5, see Table 2). This structure was described as having the best delineation at a level of about 40 to 60% ASiR. Dose reduction studies often use an ASiR level in this interval and have reported the image quality to be unchanged for the applied dose reduction.[118–120] However, in such studies knowledge about which structures may be affected by the mechanism of the ASiR algorithm at higher percentage might possibly be missed. Further in Paper I, the statistical analysis was made in comparison to 30% ASiR (Figure 10a) and all structures were rated as having worse delineation at FBP (0% ASiR; Figure 10b). In addition, the delineation of 'the cerebrospinal fluid space around the brain' at 100% ASiR was equal to that of FBP (Figure 10c and Figure 1 in Paper I). In contrast, the delineation of all the other structures tended not to deviate from each other and to increase up to 80% ASiR. Further, one of the obvious effects that limited the delineation up to a level of 60% ASiR was noise, as the delineation for all investigated anatomical structures increased up to that level (Figure 10d and Figure 1 in Paper I) and since the ASiR algorithm reduces noise. However, above 60% ASiR only the delineation described in Question 5 was rated to be worse than 30% ASiR. Hence, the delineation did not correspond to the noise reduction, but to a smoothing effect caused by the ASiR algorithm. This effect may also have influenced the overall image quality as the optimal level was identified at about 60% ASiR. The effect of the nonlinear algorithm could also be observed when profiles of 'the cerebrospinal fluid space around the brain' (the area between the skull bone and the brain tissue) were plotted, for FBP and all levels of ASiR (Figure 11). The structure was quite smooth at FBP and was sharpest at 10% ASiR. However, the structure became more and more smoothed as the level of ASiR was increased (Figure 11). The trend of Question 5 could thus be summarised as: the delineation of the structure was limited by the noise level until the nonlinear smoothing effect degraded the image quality more than the noise. It should be

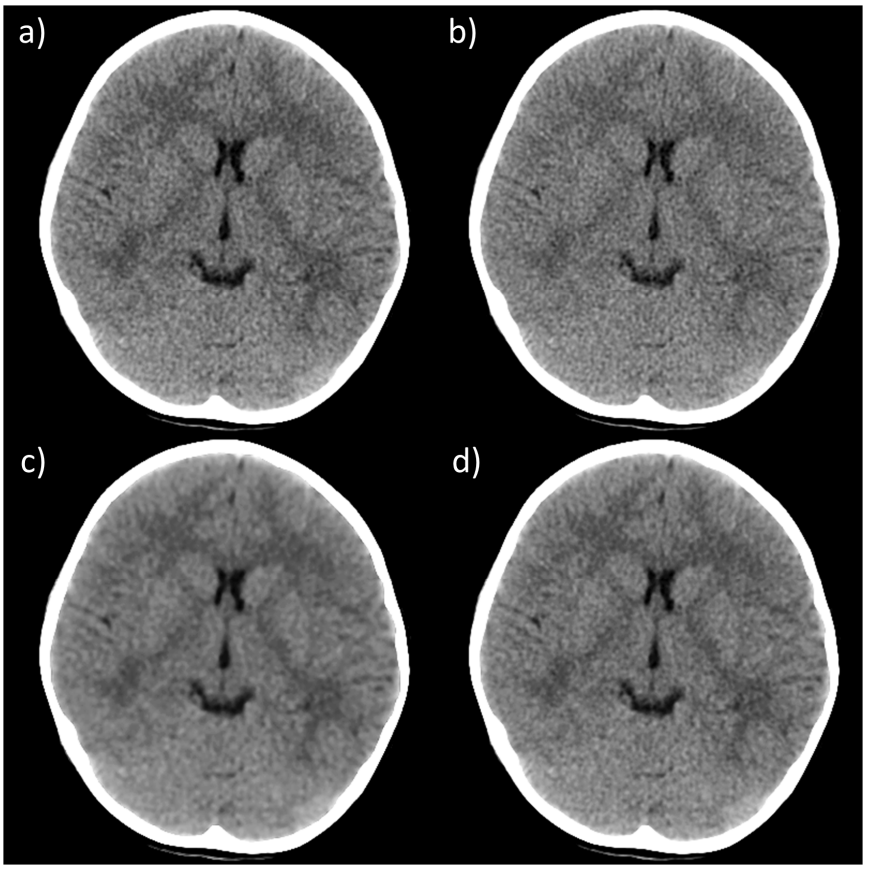

Figure 10. An example of a CT head image at four levels of ASiR, 30% (reference level; a), 0% (FBP; b), 100% (c) and 60% (optimal level; d). The question of the diagnostic value of the image quality was rated to be optimal at 60% and worst at 0% and 100% level of ASiR.

noted that the described nonlinear effect may vary on the noise level (dose level of the scan). Hence, the effect may be exceptionally prominent in this study, as the dose level of the CT examinations of the youngest paediatric patients was relatively low in comparison to other paediatric departments or hospitals.[121]

For the ASiR algorithm, the amount of noise reduction is varied by fusing a FBP image and an ASIR image. Hence, the evaluation of structures at the assessed levels of ASiR mapped how the delineation was gradually changed by the ASiR algorithm. Other studies have investigated the effect of ASiR in cerebral CT examinations both in paediatric and adult X-ray departments.[119] However, the studies have often used a smaller numbers of structures in the evaluation of the image quality such as the differentiation of grey and white matter and the overall sharpness.[118,120,121] It is also common to analyse the noise, blur and artefacts.[122]

The latter image criteria carry the risk of focussing too much on irrelevant image properties that are not to be used for the diagnosis of the patient.

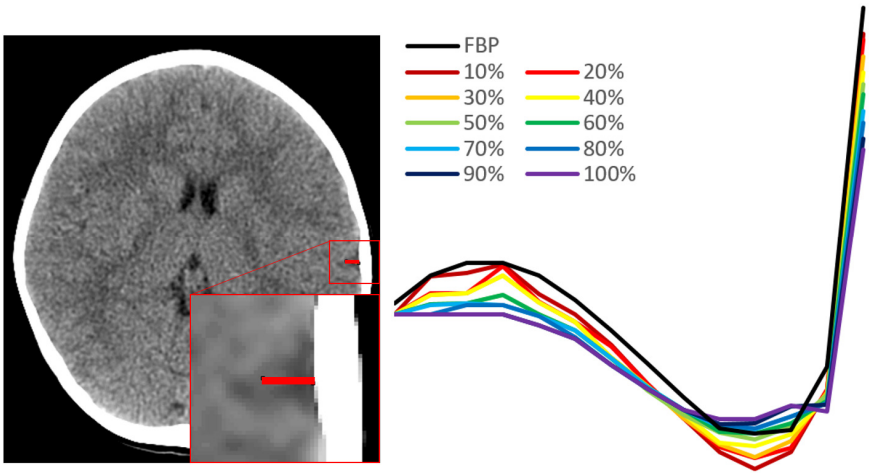

Figure 11. Illustration of the smoothing by a profile plot of 'the cerebrospinal fluid space around the brain' for each ASiR level. FBP is 0% ASiR.

4.1.2 Paediatric abdominal computed tomography (Paper II)

Strong noise reduction by nonlinear algorithms could cause the visualisation of anatomical and pathological structures to degrade. In Paper II the delineation between the liver and the abdominal wall was shown to degrade above 50% ASiR up to 100% ASiR for the convolution kernel 'Soft' (compare the images of 30% and 100% ASiR in Figure 12a and b). The visualisation of the liver has been shown by others to be a critical structure when the noise reduction strength was high for another nonlinear noise reduction algorithm.[123] Further, other studies have shown high strengths of nonlinear noise reduction to generate an unfamiliar appearance,[124] which can generate an unreliable diagnosis.

Technically, the ASiR algorithm uses an image reconstructed with FBP as the initial estimate in the iterative process. The image quality of an image reconstructed using the ASiR algorithm will thus be dependent on the applied convolution kernel. The question that described how the diagnostic value of the image quality was affected by the ASiR algorithm (Question 7) indicated a similar trend to the study in Paper I for the 'Soft' convolution kernel. A change to a more edge-enhanced kernel showed the optimal level of ASiR to change to a higher level. Even if one of the optimal combinations was 70% ASiR with a 'Standard' kernel, the image quality for the 'Standard' and 'Detail' kernel (Figure 12c and d) was never rated as superior to the optimal level of ASiR for the 'Soft' kernel (Figure 1 in Paper II). An edge enhancement will increase the appearance of the quantum noise, which could explain the correlation between the ratings of the questions and the noise level up to the optimal level of ASiR for the investigated convolution kernel. The trend of 'How well is the liver delineated against the abdominal wall?' (Question 3) for the 'Soft' kernel in Paper II was similar to Question 5 in Paper I. The shown degradation at 100% ASiR for the 'Soft' kernel was found to be reduced for the 'Standard' and 'Detail' kernel (Figure 12).

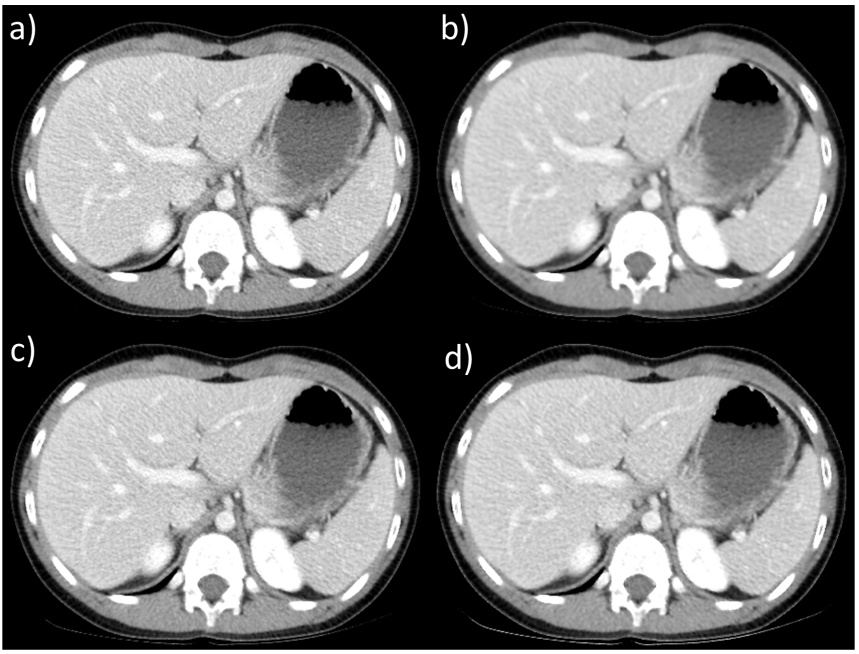

Figure 12. An example of a CT abdomen image at four of the combinations of levels of ASiR and convolution kernel, 30% and 'Soft' (reference combination; a), 100% and 'Soft' (b), 70% and 'Standard' (optimal combination; c), and 100% and 'Detail' (d).

However, 100% was the maximum level of ASiR, and the same trend might have been observed for these stronger edge-enhancing filters, if the ASiR algorithm had had stronger noise reduction. The results could thus be interpreted as: A stronger edge enhancement may compensate for the nonlinear smoothing effect shown in Paper I and II (Figure 12). However, the increased weighting of the quantum noise by these filters could concurrently reduce the delineation of structures, such that the resulting image quality is unchanged or worse. Other authors have later evaluated if the reduction in TTF by nonlinear noise reduction can be compensated for by a more edge-enhancing convolution kernel.[125] Even if that study was done on adults, the difference in noise index compared to the oldest children in Paper II (Group C, Table 1 in Paper II; NI 13.5 vs NI 34.2, after conversion to a slice thickness of 1.25 mm) indicates the noise to be considerably lower for these adults.[125] Although the assessed effect on the image quality at these two noise levels may differ, the studies indicated a similar conclusion.[125] It should also be remembered that the perceived appearance of CT images reconstructed using a nonlinear noise reduction algorithm in combination with an unfamiliar filter may differ between radiologists. Such a difference could perhaps be indicated by the relatively large span of the RP among the observers, especially for Question 7 and the 'Detail' filter (Figure 1 in Paper II; a filter not applied to any CT examinations in the paediatric department at the time of the study).

4.2 Objective effect of nonlinear noise reduction

The effects of ASiR observed in Paper I and II indicated that the image quality may be both increased and reduced by a nonlinear noise reduction algorithm and that it is dependent on the diagnostic environment (type of anatomical structure). Although the optimal noise reduction level of an algorithm could be identified using human observers, such studies may be tedious. An objective method describing the effect of a nonlinear noise reduction could be more convenient to perform. Hence, objective methods were investigated in Paper III and IV and the results from these investigations are presented in section 4.2.1 'Resolution and distortion of individual frequencies (Paper III)' and 4.2.2 'Distortion of object and noise (Paper IV)'.

4.2.1 Resolution and distortion of individual frequencies (Paper III)

The method for analysing resolution and distortion implemented in CT systems in Paper III estimated resolution using the metric PFR, which is equal to the MTF

for a linear system. The method showed that the distortion caused by the acquisition configuration was not separated from the nonlinear reconstruction algorithm, as reconstructions using the linear reconstruction algorithms FBP and SIRT both distorted the original signal due to geometrical limitations. Hence, the distortion power of the entire CT system was analysed by the method, in contrast to a previous simulation of a conventional radiological system where only the distortion caused by the nonlinear algorithm was estimated.[71] Further, the method showed a CT system using the SIRT algorithm to have slightly higher resolution and to cause slightly less distortion than a CT system using the FBP algorithm, as the same acquisition configuration was used. Hence, generation of distortion is not an indication of the CT system to be nonlinear. However, both the FBP algorithm and the SIRT algorithm did not show any dependence of the distortion on CNR whereas for the median filter and the non-negative constraint incorporated in the reconstruction the distortion was changed between CNR levels. Thus, a CNR dependence of the distortion may indicate the system to be nonlinear.

The nonlinear median filter probably exhibited aliasing distortion due to the filter kernel, which also reduced the PFR in comparison to FBP. However, the PFR increased concurrently with the noise level for the median filter. Such behaviour of an algorithm was surprising, as it might indicate that noise power has been transferred to the frequencies of the object. The complexity in analysing nonlinear noise reduction algorithms would increase if the noise was distorted to the object, which could mean that the true resolution was not estimated by the PFR. However, this was observed at very low CNRs, and the distorted power to other spatial frequencies was shown to dominate over the increased resolution for the median filter as the DI increased with decreasing CNR (Figure 3 in Paper III). Further, the observation of the distortion of the noise to the 'principle frequency' was consistent with the obtained PFR and DPS for the bilateral filter in the study of conventional radiography performed by Wells and Dobbins.[71] Hence, the relevance of the described phenomenon might be negligible, but memorable.

The non-negative constraint is often used to accommodate physical properties of radiation attenuation in the reconstruction. However, the utility of the constraint has been questioned in CT reconstruction as it could be excluded to simplify the optimisation problem.[42] The analysis of the non-negative constraint using the DI showed the distortion ratio of the system to increase as the noise level increased. In contrast to the median filter, the increased distortion for the constraint could indicate the noise power to be transferred to spatial frequencies unrelated to the object, as the PFR did not increase. Further, the PFR for the constraint showed signal power of high spatial frequencies to be affected more than lower frequencies as the noise level increased. Thus, the non-negative constraint and cut-offs due to technical limitations could lead to loss in signal power and increased distortion.

Plots of the two nonlinear noise reduction algorithms, the median and the total-variation filter, each reconstructed using FBP, showed the first one to have lower resolution (a lower PFR), distortion power (a lower DPS), and distortion index (a lower DI) at all tested 'principle frequencies' compared to the other algorithm (Figure 13). The lower PFR (resolution) of the median filter was probably due to the filter kernel. However, the distortion analysis might be surprising, as it indicates the simple median algorithm performing well in terms of keeping the distortion magnitude low. However, the DPS images showed that lower frequencies were distorted more than higher for the median filter, and for the total variation algorithm the distortion frequency distribution was the opposite, although the DI indicated the ratio between distortion and the total signal power to be less at lower frequencies for the median filter algorithm compared to the total variation. However, DPS and DI could only be used to estimate the presence of distortion and not the appearance of the distortion, which were analysed in Paper IV.

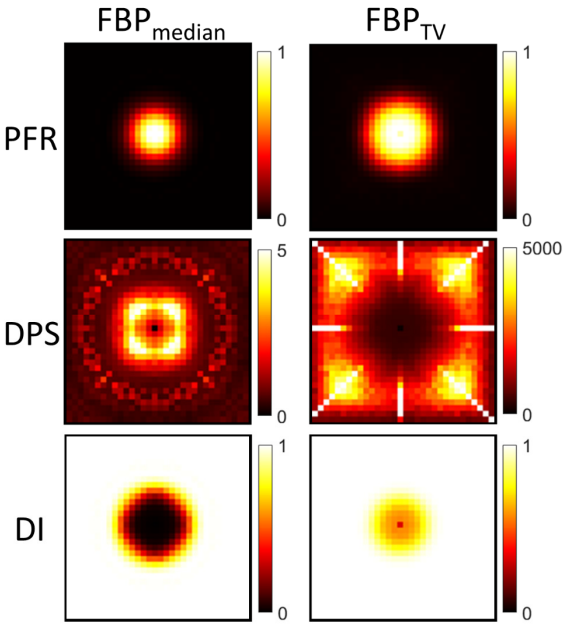

Figure 13. The "principle frequency response" (PFR; top row), distortion power spectrum (DPS; middle row), distortion index (DI; bottom row), for the two nonlinear noise reduction algorithms median filter in combination with FBP (left column), and total variation algorithm in combination with FBP (right column). Observe that the scale of the DPS image for the total variation algorithm is three magnitudes greater than for the median filter.

An objective quantitative prediction of the distortion in a CT examination is difficult to estimate. The distortion of individual spatial frequencies may not be weighted to represent the distortion of the examination. Hence, the ΣDI and $\overline{DI}$ could only be used to indicate the tendency of a nonlinear noise reduction algorithm to cause distortion in the CT image. The ratio of the distortion to the total output signal power of the system (ΣDI) for the median filter was described

as being low in comparison to the FBP or SIRT algorithm (at high CNR) and high using $\overline{\mathrm{DI}}$ (compare Figures 5a and b in Paper III). The median filter reduced the resolution and consequently also the total output signal power. Hence, the $\overline{\mathrm{DI}}$ describes the median filter to cause high distortion at individual frequencies. However, the ΣDI described the distortion of the median filter to be low, as the distortion was reduced due to the low spatial resolution of the system. Thus, the ΣDI and the $\overline{\mathrm{DI}}$ should be used in combination to compare the distortion caused by nonlinear noise reduction algorithms.

4.2.2 Distortion of object and noise (Paper IV)

In Paper III, the total distortion induced by a nonlinear noise reduction algorithm was evaluated using the DPS metric. However, in Paper IV the distortion was separated into two types of distortion, one representing the distortion of the object and the other of the noise. For a nonlinear noise reconstruction algorithm, not only the noise in the reconstructed image will be dependent on the dose of the CT scan, but also for example the image contrast. Hence, a subtraction between an image acquired at high and low dose will consist of the nonlinear distortion difference and noise, and for a linear reconstruction algorithm only noise. The noise in such an image is induced mostly by the low dose acquisition and may obscure or conceal the distortion difference. Hence, in Paper IV, the $\mathrm{NLD}_{\mathrm{object}}$ image was developed to average out the disturbing noise by visualising the systematic distortion difference (Figure 14). Intuitively, the noise power may also be distorted by a nonlinear noise reduction algorithm. Hence, in Paper IV, the $\mathrm{NLD}_{\mathrm{noise}}$ series represents the difference in reconstructing noise with and without an object present.

The nonlinear noise reduction algorithms in Paper IV were shown to transfer signal power from the object to structures correlated to the object, as the $\mathrm{NLD}_{\mathrm{object}}$ images showed structures reminiscent of the object shape. Several structures in the abdomen were seen to be affected, and the most prominently affected structure in the head was the delineation between the skull bone and the brain, i.e., 'the cerebrospinal fluid space around the brain' investigated in Paper I (Figure 14). Such distortion may be more clinically disturbing than a distortion of stochastic variations. Hence, a distortion that mimics the object may affect the resolution or induce structures that could be interpreted as pathology. In contrast, a nonlinear noise reduction algorithm that only induced distortion of stochastic variations would probably be able to be approximated as linear, as the distortion would be interpreted as extra noise. Few visible structures in difference images between

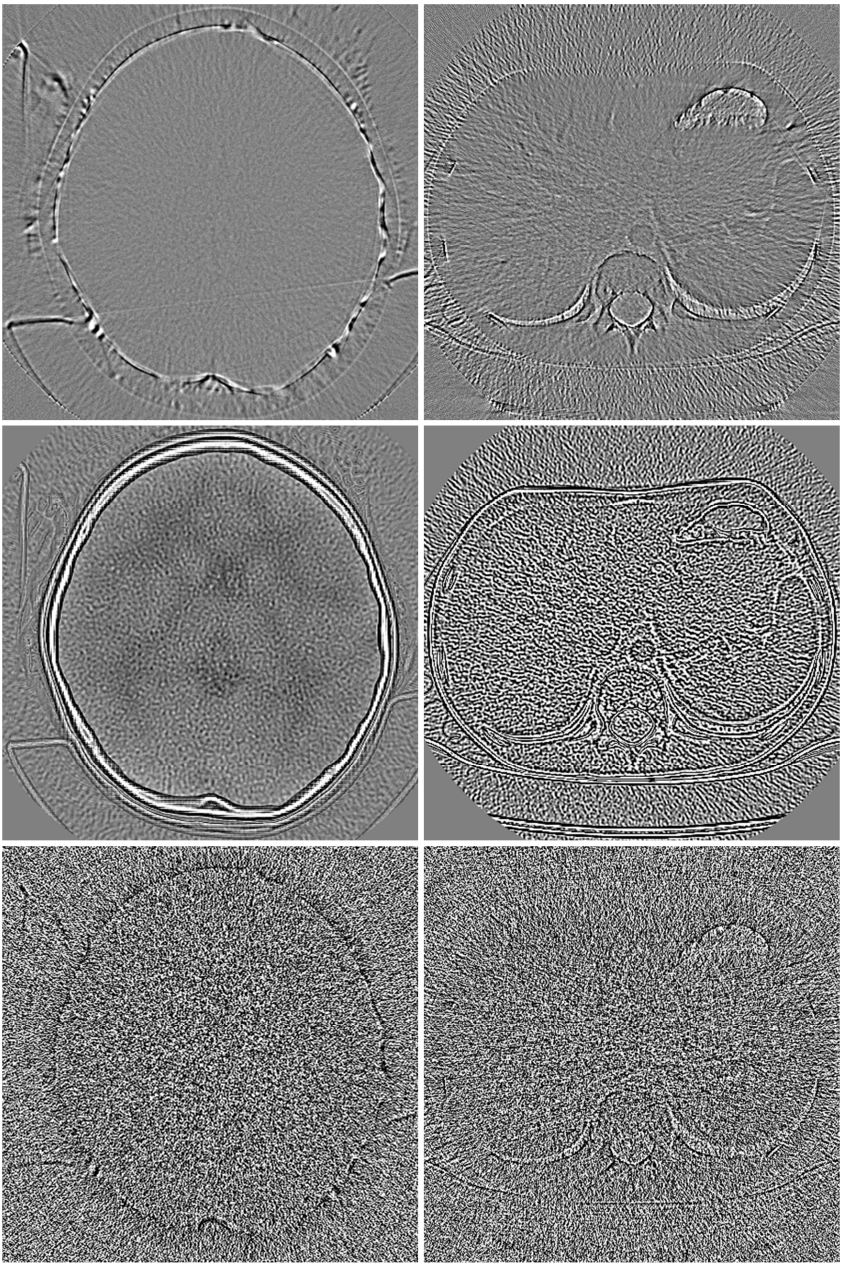

Figure 14. Shows a typical cerebral (left column) and a typical abdominal (right column) CT examination. NLD_{object} images (top row) show the distortion of the total variation algorithm, the difference images between ASiR 100% and FBP (middle row) show the difference between ASiR and FBP, difference images between the total variation algorithm and FBP with added noise (low dose; bottom row) show the noise to obscure the differences between the algorithms.

images reconstructed using FBP and a noise reduction algorithm are sometimes given as proof that the algorithm preforms well;[76] as discussed previously, this may be true for that specific noise level and if the noise in the difference image is low enough to not hide the structures (Figure 14). In an optimisation evaluation situation, the systematic nonlinear distortion difference between two noise levels could be visualised without the presence of noise using the NLD_{object}. For those interested in such analysis without having access to manipulation of the projection data, the NLD'_{object} may be generated by acquiring images of the same object several times at the two noise levels of interest. Further, the images of each noise level are then averaged and compared to each other by subtraction. Remember that the NLD'_{object} might show the nonlinear difference of, for example, the size of the focus spot or number of projections acquired, which might be useful in the optimisation situation. In contrast, the NLD_{object} will isolate the performance of the nonlinear noise reduction algorithm, which may instead be more helpful for algorithm engineers in the optimising process of the noise reduction algorithm itself.

The type of nonlinear noise reduction was shown to transfer the noise power differently, as the magnitude of the pixel values was low in the NLD_{noise} series for the median filter compared to the total variation algorithm (Figure 15). Although the distortion of the noise caused by the median filter was low, it consisted of both stochastic variation and structures correlated to the object, especially for the skull bone of the head at high noise (Figure 15) and for some abdominal structures (Figure 6 in Paper IV). The latter distortion type would possibly confirm the observed tendency of the increased PFR as the CNR was reduced, in Paper III. Although such an increase in PFR might be beneficial, the NLD_{noise} series should instead be used to identify if the transferred noise power could have generated structures correlated to the object. Thus, the lack of such correlation in both the NLD_{object} image and NLD_{noise} series could perhaps indicate the nonlinear noise reduction algorithm being approximated as linear. However, the presence of anatomical structures in these images could be used to locate structures to investigate in human observer studies in order to possibly reduce the evaluation time and focus on relevant structures.

It is always preferable if an algorithm causes low distortion, i.e. transfers as low signal power to other frequencies as possible. However, the low distortion may be expressed more unfavourably than a higher distortion. For example, a stochastic distribution of the distortion would have only generated an extra noise to the image in contrast to a distribution correlated to the object. Hence, the distortion in images of patients must be analysed to evaluate the degradation of the clinical image quality caused by a nonlinear noise reduction algorithm. An assessment using the proposed methods in Paper IV on patients should

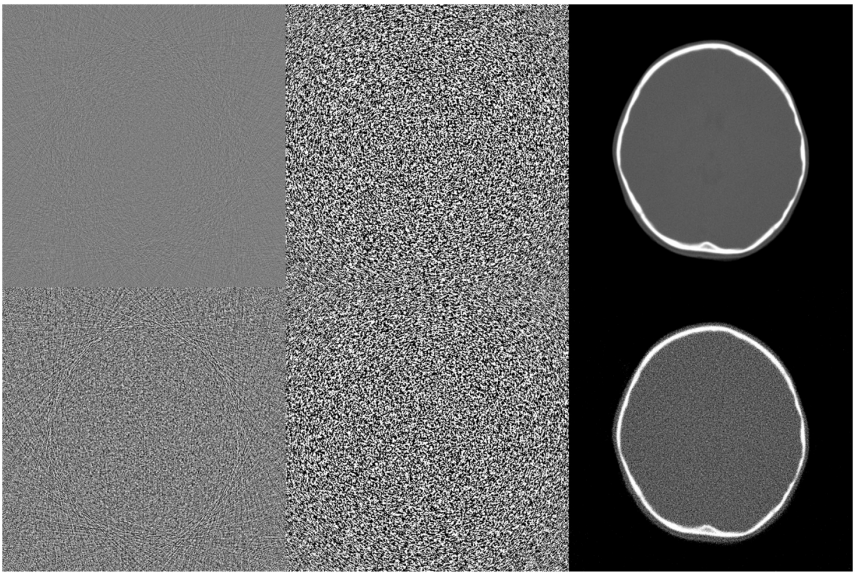

Figure 15. The nonlinear distortion of noise (NLD_{noise}) of a typical CT head examination. Two simulated noise levels, one with eight times lower noise (top row) than the other (bottom row), were calculated for the median filter (left column) and the total variation filter (middle column) using FBP. A reconstruction of each noise level for comparison (right column).

theoretically be possible but is clearly not convenient or appropriate for conventional CT system. Further, the assessment would be limited to body parts that can be fixed, i.e. not subject to respiratory, cardiac or peristaltic motion. However, new photon-counting CT systems may have the possibility to integrate the acquisition over different time intervals to generate NLD_{object} and NLD_{noise} images using one acquisition. Hence, each time interval will represent a repetition of the lower dos acquisition. The generation of the NLD_{noise} images would still require access to the projection domain. Nonetheless, in conventional CT systems, anthropomorphic phantoms may be sufficient to use when investigating the effects of nonlinear noise reduction algorithms on anatomical structures and/or pathology.

Nonlinear noise reduction algorithms are sometimes compared to FBP by a difference image.[76] Although FBP is a linear reconstruction technique, such an image will not show the nonlinear distortion but the difference between the reconstruction techniques. Further, the image will be contaminated by noise as FBP does not solely reduce noise, especially when the CT examinations are acquired at low doses (Figure 14). Furthermore, the difference between two algorithms could be zero in specific conditions, i.e. the spatial resolution induced by a nonlinear noise reduction algorithm may be the same as for a smoothing

convolution kernel. Hence, an analysis of the distortion of a nonlinear algorithm is best performed with the same algorithm.

The images NLD_{object} and NLD_{noise} enabled a closer analysis of the distortion effect caused by nonlinear algorithms and could increase the understanding of how the distortion is expressed. Further, the distortion was aimed to be visualised at the corresponding locations in the image, such that it would be easy to track and understand it intuitively. Furthermore, the method to generate an NLD_{object} image requires access to perform averaging and take the difference between the projection data. Thus, an analysis of nonlinear algorithms on CT systems without this type of access may be done using the NLD'_{object}, which is an approximation of the NLD_{object} (Figure 16). The difference between the NLD_{object} and NLD'_{object} is noise, since the noise in an acquisition of the high dose image for the NLD'_{object} is not correlated with the noise acquired in the images of low dose. This is in contrast to NLD_{object}, where the exact same noise was compared to estimate the distortion. However, for the highest evaluated CNR in Paper IV 128 repetitions were required to generate an NLD'_{object} comparable to the NLD_{object} (Figure 16), which can be completed within the time of a working day.

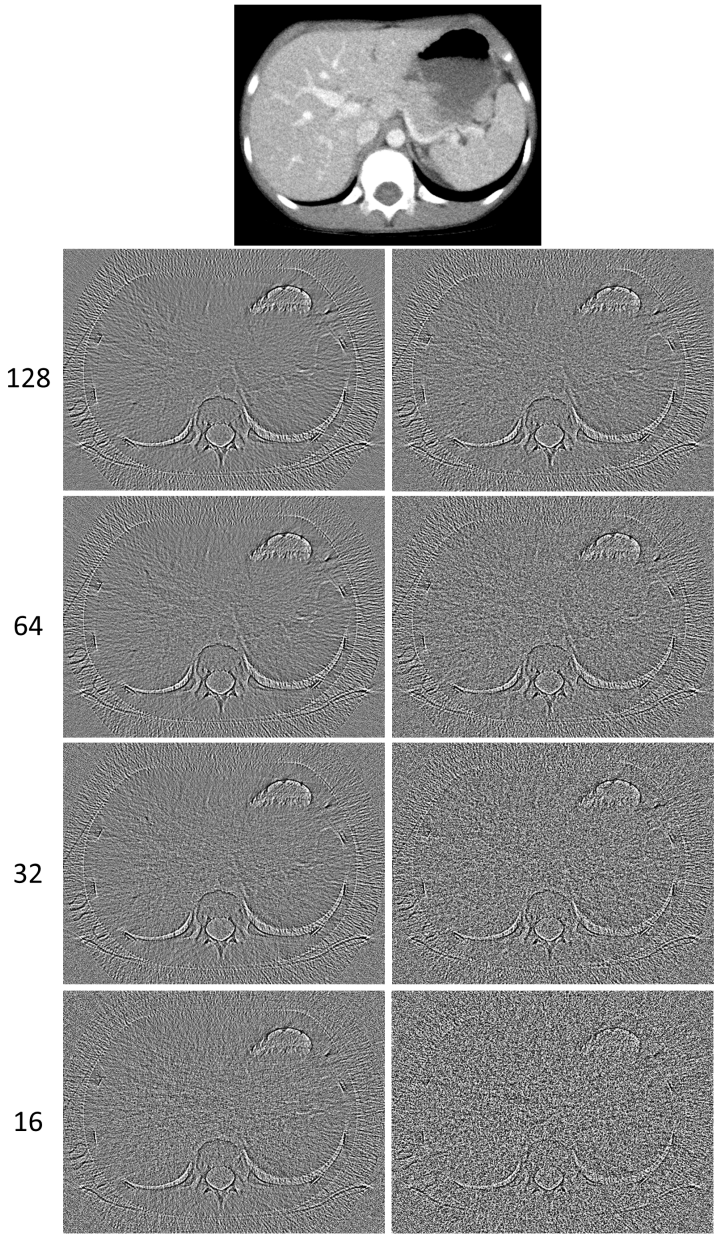

Figure 16. A typical CT abdomen image with added noise (top image), nonlinear distortion of object (NLD_{object}; left column) and the approximated nonlinear distortion of object (NLD'_{object}; right column) of the same image calculated using 128, 64, 32, and 16 images (top to bottom) respectively.

4.3 General discussion

The overall aim of the thesis was to investigate the effects of nonlinear noise reduction algorithms in CT. Besides the obvious effect of reducing noise, the results from the thesis indicate that a nonlinear noise reduction algorithm may increase the image quality to a limited level. Further, using the definition of distortion from the present thesis, i.e. transfer of signal power to other frequencies, the distortion can be interpreted as the source of all the image quality changes caused by the nonlinear noise reduction algorithm. The induced distortion of a nonlinear noise reduction algorithm may be divided into distortion of the object and distortion of the noise. Furthermore, the maximum image quality induced by such an algorithm is obtained at as low noise as possible and will most likely be reduced as the noise level is increased. These statements can summarise the investigated effects of nonlinear noise reduction algorithms in CT systems.

Noise reduction algorithms are often distributed with several levels indicating the amount of noise reduction. Finding the optimal level of a noise reduction algorithm may require that all these levels are evaluated. In Paper I and II, the number of cases to be evaluated for the ASiR algorithm would have been equal to the number of patients multiplied by the ten levels of ASiR. Further, the time of evaluation for each observer increases proportionally to the evaluated noise reduction levels. Nevertheless, although the number of patients was relatively few in Paper I and II, the number of levels was decided to be reduced (Table 1) as the evaluation time for the observers would have been unreasonable if all levels were included in the study. Furthermore, in Paper I, the optimal level was originally not thought to be found above 60% ASiR due to the first impression of the ASiR images. Thus, not all levels of ASiR were included in the evaluation in Paper I. It is fairly common to not evaluate every level of the noise reduction algorithms in observer evaluation studies.[126–128] This reduction of the number of levels increases the risk of missing the optimal level. The study of the oldest patients in Paper I (Group A, Table 1 in Paper I) indicated this risk and the investigated levels of ASiR were shifted and extended to higher levels in the study of the other age groups. From the latter study the optimal level was indicated not to have been missed for the oldest age group. A larger number of patients could potentially have given a more certain result. However, the obtained trends were quite clear and the evaluated number of patients was similar to other observer studies of noise reduction algorithms.[129,130] Further in Paper I, the effect of ASiR on the image quality was indicated to be quite subtle between the levels. The effect was assumed to not be very different between examination types. Hence, the chosen levels of ASiR were distributed more sparsely in the study of the abdominal CT examinations (Paper II). The optimal level of ASiR was evaluated mainly by the

question of the diagnostic value of the image quality (Question 7 in both studies; Table 2), as Question 7 summarised the general effect of ASiR on image quality well. An indication of this is that the pooled delineation of all anatomical structures would have indicated 80% ASiR to be the optimal level in Paper I. Hence, the degradation of 'the cerebrospinal fluid space around the brain' was shown to be considered when Question 7 was rated. Besides helping the observer to evaluate the image quality by forcing them to rate specific structures, the questions of the anatomical structures could potentially be used in the optimisation of other than the standard scanning protocol.

A linear noise reduction algorithm reduces noise relatively homogeneously over the image, i.e. independently of the noise level or the imaged object. Increased smoothing using linear convolution kernels will increase the visibility of anatomical structures until the delineation of important structures is too low, when the increase in image quality obtained by reduction in noise can no longer compensate for the degradation in image quality caused by the reduction in spatial resolution. The nonlinear ASiR algorithm also increases image quality by reducing the noise, and the reduction is often estimated in an image of a water phantom. However, the increase in diagnostic image quality does not have to be proportional to the reduced noise estimated in the water phantom, as the algorithm is nonlinear and can reduce noise dependent on the anatomical structure as well as noise level.[131] Further, like a convolution kernel, the nonlinear ASiR algorithm may also degrade the spatial resolution. By the same reasoning, the degradation does not have to be the same for all anatomical structures. Furthermore, unlike the convolution kernel, the spatial resolution may be reduced as the absorbed dose is reduced and the reduction may also be disproportionate to dose reduction. Even though the task-based metric TTF describes the changes in resolution of sharp edges well,[64] it is possible that the resolution may be affected differently between various textures. Hence, for nonlinear systems, an assessment of the visibility of anatomical structures is crucially important to detect deviating effects of the reconstruction.

The questions related to the delineation of the anatomical structures in the observer evaluation studies worked well to identify structures that had been affected by the nonlinear ASiR algorithm. Due to the nonlinear behaviour of the ASiR algorithm it was also important to remember that the assessed image quality was only valid for the used noise level. Further, the observations of the subtle difference in general image quality between the ASiR levels indicated that a possible dose reduction should be carefully conducted. Hence, the suggested dose reduction made by some CT systems is often based on the standard deviation of the CT number estimated in an image of a cylindrical water phantom and may possibly not be in proportion to the induced image quality in clinical patients. This

statement is strengthened by phantom studies of nonlinear noise reduction algorithms that have shown the resolution and noise power spectrum to reduce differently between materials as the dose is reduced.[132–134]

Noise reduction algorithms such as the ASiR algorithm investigated in Papers I and II are nonlinear, as a regularization step is used to remove noise.[15,135] The nonlinear effect on image quality was proposed to originate from the distortion caused by the noise reduction algorithm. The distortion effect had been investigated in conventional radiology, and the method of analysing distortion was implemented in CT in Paper III. Implemented in CT, the method described the total distortion caused by both the acquisition system and the reconstruction system (including the noise reduction). However, the distortion was analysed for sinusoids and could not be generalised to clinical CT images. Hence, in Paper IV a new method was developed to investigate distortion in clinical images. The studies in Paper III and IV investigated relative basic nonlinear algorithms, as the purpose was to understand what the implemented and develop methods could show. For example, the nonlinear noise reduction algorithms were reducing the noise in the projection domain and not integrated in the updating procedure of the IRTs. However, it was found in Paper IV that the distortion induced by a nonlinear noise reduction algorithm investigated in Paper III consisted of distortion of both the object and the noise. Further, the method excluded the distortion caused by the CT acquisition system and concurrently separated the distortion of the object from the distortion of the noise. Furthermore, the resulting distortion was shown to consist of stochastic variation and structures reminding of the object. As long as the nonlinear noise reduction algorithm only induces distortion of stochastic variations, the system should be considered as linear. However, it may still be possible to consider a system to be linear with a small amount of distortion power correlated to the imaged object, which must be further investigated. Even if the whole CT system can be considered as linear, an image quality different from the one obtained using the traditional FBP reconstruction might still have a psychological effect on the radiologist. This effect is not within the scope of the present thesis and has yet to be investigated. However, optimisation of noise reduction algorithms has already focused on mimicking the appearance of the image quality obtained from FBP to accommodate this potential effect.[76]

Dose reduction using nonlinear noise reduction algorithms has been shown to be possible in many radiological fields of CT imaging.[118–120,136–138] However, the evaluation of image quality of nonlinear algorithms is complex, as the imaging properties of these algorithms are not as predictable as for linear algorithms. It would thus be preferable if the changes in image quality induced by a nonlinear noise reduction algorithm could be traced and predicted in a similar way as for a linear system to be able to safely reduce the absorbed dose from CT examinations.

A report from the AAPM suggests using task-based metrics to evaluate the performance of new CT systems.[72] Hence, the task group assumes that nonlinear noise reduction algorithms could be approximated as linear. Such an assumption may be risky, as these recommended metrics ignore the fact that distortion effects induced by a nonlinear algorithm may differ between reconstructed objects. For example, the distortion obtained in the estimation of the resolution using the TTF, i.e. induced by a sharp edge, could not be assumed to be valid generally. Hence, the resolution must be estimated in the anatomical environment of the diagnostic task to better account for the distortion effects of the nonlinear noise reduction.[71] The TTF and NPS has recently been modified to estimate the detectability of lesions in patient images, which indicated slight differences between phantom-derived detectability and patient-derived detectability.[81,82] Even though the difference was not significant in this type of detection task, the study indicated the importance of evaluating image quality from nonlinear noise reduction in a clinical context.[81] These modified metrics could probably be used to predict image quality changes for specific diagnostic tasks in order to reduce absorbed dose to the patient. In contrast, the knowledge derived from the present thesis may potentially help in understanding the cause and appearance of the effect from nonlinear noise reduction algorithms.

5. Conclusions

The effect of a nonlinear noise reduction algorithm on the diagnostic image quality was investigated in both paediatric cerebral and abdominal CT imaging. The latter study also investigated the dependence of the diagnostic image quality of the same nonlinear noise reduction algorithm on the type of convolution kernel. The use of nonlinear noise reduction algorithms in clinical CT imaging was indicated as inducing potential benefits of the perceived image quality for several anatomical structures. However, nonlinear noise reduction should be carefully implemented as the diagnostic image quality may be affected by nonlinear smoothing. Thus, the delineation of relevant structures in the images of CT examinations should be investigated to ensure that a satisfactory effect is achieved by implementation. The delineation of 'the cerebrospinal fluid space around the brain' and 'the liver delineation against the abdominal wall' for cerebral and abdominal CT examinations respectively is shown to be affected negatively. Hence, these specific anatomical structures should be of concern in future development of nonlinear noise algorithms.

Concerning nonlinear noise reduction algorithms which may be combined with different convolution kernels, a more edge-enhancing convolution kernel may be used to compensate for the smoothing of noise reduction. However, the increase in the perceived noise by the convolution kernel may be the limiting factor for image quality. Hence, image quality may still be equal to another combination of convolution kernel and nonlinear noise reduction algorithm.

Using human observers as a tool to evaluate nonlinear noise reduction algorithms works well and is found to induce clear trends of the diagnostic image quality to the level of the nonlinear noise reduction for both cerebral and abdominal CT examinations. Despite the tedious process, human observers should be included in an evaluation of nonlinear noise reduction algorithms to analyse the psychophysical aspect and account for differences in the opinion of radiologists. This aspect is of great concern as the perceived image quality of a nonlinear noise-reduced image may be unfamiliar to the radiologist and may affect ability to detect and diagnose.

The metrics developed for resolution and distortion effect analysis in conventional radiology were implemented in nonlinear CT imaging. These objective metrics indicated the effects of nonlinear noise reduction algorithms on the image quality being caused by distortion. The distortion was dependent on the composition of the imaged object, and the distortion power might increase as the level of noise is increased. Further, the tendency of a nonlinear noise reduction

algorithm to cause distortion can be assessed by separating the spatial resolution (PFR) from the distortion (DPS) by analysing the response of the algorithm on sinusoids. Two ratios between the distortion power and the total output power (ΣDI and $\overline{\text{DI}}$) may be used in combination to compare the distortion caused by nonlinear algorithms.

A method was developed to visualise the distortion of object and noise caused by a nonlinear noise reduction algorithm in CT imaging. The distortion of the imaged object and the noise was analysed separately by the developed images ($\text{NLD}_{\text{object}}$ and $\text{NLD}_{\text{noise}}$) visualising the location of distorted structures. Thus, an analysis of the distortion should be considered if nonlinear noise reduction algorithms are to be used for a reduction of absorbed dose in CT imaging.

6. Future Perspectives

An analysis of the effects of nonlinear noise reduction on image quality is complex and requires considerable attention. Here are a few examples of subjects that could be further investigated:

- *Distortion analysis of clinical nonlinear noise reduction algorithms*. The performance of a nonlinear noise reduction algorithm is often compared to FBP and visualised in a subtraction image. Such an image does not present the distortion of the nonlinear algorithm, but the difference between the algorithms covered in noise as FBP does not reduce noise. In the present thesis, the nonlinear effect on image quality in existing systems has only been approximately estimated by NLD'_{object}, since manufacturers are often reluctant to provide full access to the projection data. Hence, analysis of the distortion using NLD_{object}, NLD_{noise}, PFR, DPS, DI, ΣDI and $\overline{DI}$ has yet to be tested.

- *Approximation of nonlinear systems*. No imaging system is strictly linear. However, a CT system using FBP can be approximated as linear and analysed using metrics of the theory of linear systems. This approximation has been shown to be invalid for nonlinear noise reduction algorithms, as resolution and noise vary with the object and noise level. The observed variations have been approximated to follow a linear relationship, such that the metrics can be modified to be task-specific. These metrics have been shown to be useful in estimating image quality in many cases. However, a nonlinear system could induce effects on image quality, which invalidates the approximation. Hence, criteria are needed to determine when a linear approximation of a nonlinear noise reduction algorithm is suited. The present thesis has developed methods analysing distortion, which may be one of the criteria.

- *Training of a neural network*. Deep learning has been used to develop noise reduction algorithms, where a neural network is trained through comparisons between high and low noise images of the same object. A temporarily noise-reduced image is compared to the low noise image to find differences which can be used to fine-tune the parameters in the noise-reducing neural network. To our knowledge, a neural network has never been trained to reduce the difference obtained by the images of NLD_{object} and NLD_{noise}, which may perhaps reduce the distortion caused by the algorithm at high noise levels.

Acknowledgements

Denna avhandling hade inte blivit till utan hjälp och stöd från personer i min närhet. Ord kan inte fullt ut beskriva min tacksamhet till er, men förhoppningsvis kan de ge er en antydan till den betydelse som ni haft i mina forskningsstudier.

Först vill jag tacka min huvudhandledare **Anne Thilander-Klang**, du som vågade ta dig an mig och göra mig till den forskare jag är idag. Du skapar alltid ett så fint och öppet samtalsklimat där det känns tryggt att dela alla tankar och idéer. Tack även för alla gånger du stöttat mig när jag tvivlat på min egen förmåga.

Självklart vill jag också tacka min biträdande handledare **Magnus Båth**, för den tid och det engagemang du lagt ner på att hjälpa mig med de problem som jag stött på under mina doktorandstudier. Du har alltid sporrat mig till att göra mitt yttersta och samtidigt hjälpt mig att inte tappa modet när arbetet varit motigt.

Till er på röntgenavdelning vid drottning Silvias barn och ungdomssjukhus som bistått i delarbetena. **Fredrik Stålhammar, Håkan Boström, Håkan Caisander**, **Jenny Ahlin**, **Lars-Martin Wiklund**, **Liz Ivarsson** och **Mats Jönsson,** tack för att ni bidrog med expertkunskaper då ni granskade bildmaterialet till delstudierna, men även **Eira Stokland** som avsatte tid till er. **Berit Trens,** tack för den glädje du spridit och all den hjälp jag fått från dig vid datortomografen då jag skulle bereda bildmaterialet. Detsamma gäller dig **Siw Johansson,** även fast du inte kan bevittna den färdigställda avhandlingen, så kommer du att finnas kvar i mitt minne som en underbar människa.

Tack till alla mina doktorandrumskamrater som jag haft under åren som jag flyttat runt från rum till rum, **Johan Spetz**, **Emil Schüler**, **Jenny Nilsson**, **Daniela Marocsan**, **Rimon Thomas**, **Kerstin Ledenius**, **Angelica Svalkvist**, **Maral Mírzai**, **Christina Söderman**, **Christian Waldenberg** och alla andra doktorandkamrater. Tack till alla andra på radiofysik (Medicinsk strålningsvetenskap), som hjälpt mig och ett speciellt tack till **Kerstin Lagerstrand** och **Tobias Rydén** för att ni lånade ut era datorer till mig så att jag kunde genomföra mina simuleringar.

Thank you to **Jered Wells** and **James T. Dobbins III** for inspiring me to investigate the distortion of nonlinear algorithms, without your paper Paper III and IV in this thesis would never have been written.

Till mina kära kollegor i NU-sjukvården som varje dag förgyller mitt arbete som sjukhusfysiker, **Sara Asplund**, **Louise Strandberg**, **Olivia Carlstein** och **Andreas Österlund**, tack även för alla goda samtal och stöttande ord när det känts svårt och tungt med forskandet. **Lea Sillfors-Elverby** och **Johnny Kallin** även om vi inte arbetar tillsammans nu så har ni också länge förgyllt mina arbetsdagar. Tack även till alla mina chefer som jag haft och till min nuvarande, **Morgan Persson,** tack för att ni varit så tillmötesgående och tillåtit mig fullfölja mina doktorandstudier.

Ett speciellt tack vill jag rikta till **Roland Eklöf**, du var min förebild att börja forska och kallades ibland för professorn, jag vet fortfarande inte om du var det, men låt mig tro att det var så.

Sist men absolut inte minst så vill jag tacka min familj. **Cecilia**, tack för att du hjälpt mig att skriva denna doktorsavhandling genom att vara den bästa fru man kan tänka sig. **Alfred** och **Algot** tack för att ni har fått mig att tänka på annat när jag tänkt för mycket på förvrängda röntgenbilder. Att få leva livet tillsammans med er är en så otroligt stor gåva! Tack även mamma **Ingrid** och pappa **Dan** samt mina svärföräldrar **Gunilla** och **Lars** för att ni kommit och stöttat familjen då det behövts.

This work was supported by grants from the King Gustav V Jubilee Clinic Cancer Research Foundation, the Swedish Radiation Safety Authority (SSM) and the Department of Research and Development at the NU Hospital Group.

References

1. Beckmann EC. CT scanning the early days. Br J Radiol. 2006;79(937):5–8.
2. Hounsfield GN. Computerized transverse axial scanning (tomography): part 1. Description of system. Br J Radiol. 1973;46(552):1016–22.
3. United nations scientific committee on the effects of atomic radiation (UNSCEAR). Sources and effects of ionizing radiation Volume I: sources. UNSCEAR report to the General Assembly, with Scientific Annexes. 2000.
4. Almén A, Richter S, Leitz W. Radiologiska undersökningar i Sverige under 2005. 2008. SSI report: 2008:03 *in Swedish.* ISSN 0282-4434.
5. Thilander Klang A. Utveckla metoder för bestämning av diagnostiska standarddoser och dosreferensnivåer för DT-undersökningar av barn. 2017. SSM report 2017:06 *in Swedish.* ISSN: 2000-0456.
6. Almén A, Lars J. Radiologiska undersökningar i Sverige under 2018. 2020. SSM report 2020:14 *in Swedish.* ISSN: 2000-0456.
7. Preston DL, Shimizu Y, Pierce DA, Suyama A, Mabuchi K. et al. Studies of mortality of atomic bomb survivors. Report 13: solid cancer and noncancer disease mortality: 1950-1997. Radiat Res. 2012;178(2):381–407.
8. Ozasa K, Shimizu Y, Suyama A, Kasagi F, Soda M, Grant EJ, et al. Studies of the mortality of atomic bomb survivors , Report 14 , 1950 – 2003 : an overview of cancer and noncancer diseases. Radiat Res. 2012;243(3):229–43.
9. ICRP, 2007 The 2007 Recommendations of the international commission on radiological protection. ICRP Publication 103. Ann ICRP 37 2–4.
10. Strålsäkerhetsmyndighetens föreskrifter om allmänna råd om medicinska exponeringar. 2018 SSMFS 2018:5 *in Swedish*. ISSN: 2000-0987.
11. ICRP, 2007. Radiological protection in Medicine. ICRP Publication 105 Ann ICRP 37 (6).

12. McCollough CH, Chen GH, Kalender W, Leng S, Samei E, Taguchi K, et al. Achieving routine submillisievert CT scanning: report from the summit on management of radiation dose in CT. Radiology. 2012;264(2):567–80.

13. Gordon R, Bender R, Herman GT. Algebraic reconstruction techniques (ART) for three-dimensional electron microscopy and X-ray photography. J Theor Biol. 1970;29(3):471–81.

14. Brooks RA, Di Chiro G. Principles of computer assisted tomography (CAT) in radiographic and radioisotopic imaging. Phys Med Biol. 1976;21(5):689–732.

15. Hsieh J. Computed tomography: principles, design, artifacts, and recent advances. 2nd ed. Bellingham, Washington USA: SPIE and John Wiley & Sons, Inc.; 2009. (SPIE Press Monograph).

16. Thibault J-B, Sauer KD, Bouman CA, Hsieh J. A three-dimensional statistical approach to improved image quality for multislice helical CT. Med Phys. 2007;34(11):4526–44.

17. May MS, Wüst W, Brand M, Stahl C, Allmendinger T, Schmidt B, et al. Dose reduction in abdominal computed tomography: Intraindividual comparison of image quality of full-dose standard and half-dose iterative reconstructions with dual-source computed tomography. Invest Radiol. 2011;46(7):465–70.

18. Hwang HJ, Seo JB, Lee HJ, Lee SM, Kim EY, Oh SY, et al. Low-dose chest computed tomography with sinogram-affirmed iterative reconstruction, iterative reconstruction in image space, and filtered back projection: Studies on image quality. J Comput Assist Tomogr. 2013;37(4):610–7.

19. Persson M, Grönberg F. Bias-variance tradeoff in anticorrelated noise reduction for spectral CT. Med Phys. 2017;44(9):e242–54.

20. Huang JY, Kerns JR, Nute JL, Liu X, Balter PA, Stingo FC, et al. An evaluation of three commercially available metal artifact reduction methods for CT imaging. Phys Med Biol. 2015;60(3):1047–67.

21. Katsura M, Sato J, Akahane M, Kunimatsu A, Abe O. Current and novel techniques for metal artifact reduction at CT: practical guide for radiologists. Radiographics. 2018;38(2):450–61.

22. Wayer DR, Kim NY, Otto BJ, Grayev AM, Kuner AD. Unintended consequences: review of new artifacts introduced by iterative reconstruction CT metal artifact reduction in spine imaging. Am J Neuroradiol. 2019;40(11):1973–5.

23. Rousselle A, Amelot A, Thariat J, Jacob J, Mercy G, De Marzi L, et al. Metallic implants and CT artefacts in the CTV area: where are we in 2020? Cancer Radiother. 2020;24(6–7):658–66.

24. Pettersson E, Bäck A, Björk-Eriksson T, Lindencrona U, Petruson K, Thilander-Klang A. Structure delineation in the presence of metal – a comparative phantom study using single and dual-energy computed tomography with and without metal artefact reduction. Phys Imaging Radiat Oncol. 2019;(9):43–9.

25. Pettersson E, Bäck A, Thilander-Klang A. Comparison of metal artefacts for different dual energy CT techniques. Radiat Prot Dosimetry. 2021;195(3–4):232–45.

26. De Man B, Nuyts J, Dupont P, Marchai G, Suetens P. Reduction of metal streak artifacts in x-ray computed tomography using a transmission maximum a posteriori algorithm. IEEE Trans Nucl Sci. 2000;47(3):977–81.

27. Xu J, Tsui BMW. Electronic noise modeling in statistical iterative reconstruction. IEEE Trans image Process. 2009 Jun;18(6):1228–38.

28. Whiting BR. Signal statistics in x-ray computed tomography. In: Antonuk LE, Yaffe MJ, editors. Medical Imaging 2002: Physics of Medical Imaging. SPIE; 2002. p. 53–60.

29. Dobbins III JT. Image quality metrics for digital systems. In: Van Metter RL, Jacob B, Kundel HL, editors. Handbook of Medical Imaging. Bellingham, Washington USA: Society of Photo-Optical Instrument Engineers; 2000. p. 161–222.

30. Faulkner K, Moores BM. Analysis of x-ray computed tomography images using the noise power spectrum and autocorrelation function. Phys Med Biol. 1984;29(11):1343–52.

31. Boedeker KL, Cooper VN, McNitt-Gray MF. Application of the noise power spectrum in modern diagnostic MDCT: part I. Measurement of noise power spectra and noise equivalent quanta. Phys Med Biol. 2007;52(14):4027–46.

32. Boedeker KL, McNitt-Gray MF. Application of the noise power spectrum in modern diagnostic MDCT: part II. Noise power spectra and signal to noise. Phys Med Biol. 2007;52(14):4047–61.

33. Solomon JB, Christianson O, Samei E. Quantitative comparison of noise texture across CT scanners from different manufacturers. Med Phys. 2012;39(10):6048–55.

34. Chen B, Christianson O, Wilson JM, Samei E. Assessment of volumetric noise and resolution performance for linear and nonlinear CT reconstruction methods. Med Phys. 2014;41(7):071909.

35. Samei E, Richard S. Assessment of the dose reduction potential of a model-based iterative reconstruction algorithm using a task-based performance metrology. Med Phys. 2015;42(1):314–23.

36. Judy PF, Swensson RG, Szulc M. Lesion detection and signal-to-noise ratio in CT images. Med Phys. 1981;8(1):13–23.

37. Hussein EMA. Computed radiation imaging: physics and mathematics of forward and inverse problems. Elsevier Science London Waltham; 2011.

38. Saat S, Nguang SK, Nasiri A. Analysis and synthesis of polynomial discrete-time systems: an SOS approach. Butterworth-Heinemann Elsevier Oxford Cambridge; 2017.

39. Beister M, Kolditz D, Kalender WA. Iterative reconstruction methods in x-ray CT. Phys Medica. 2012;28(2):94–108.

40. Cierniak R. X-Ray Computed tomography in biomedical engineering. Springer London; 2011. p. 248–264.

41. Elbakri IA, Fessier JA. Segmentation-free statistical image reconstruction for polyenergetic x-ray computed tomography with experimental validation. Phys Med Biol. 2003;48(15):2453.

42. Haase V, Hahn K, Schöndube H, Stierstorfer K, Maier A, Noo F. Impact of the non-negativity constraint in model-based iterative reconstruction from CT data. Med Phys. 2019;46(12):e835–54.

43. Kachelriess M, Watzke O, Kalender WA. Generalized multi-dimensional adaptive filtering for conventional and spiral single-slice, multi-slice, and cone-beam CT. Med Phys. 2001;28(4):475–90.

44. La Riviere PJ, Pan X. Nonparametric regression sinogram smoothing using a roughness-penalized Poisson likelihood objective function. IEEE Trans Med Imaging. 2000;19(8):773–86.

45. La Rivière PJ. Penalized-likelihood sinogram smoothing for low-dose CT. Med Phys. 2005;32(6):1676–83.

46. Moscariello A, Takx RAP, Schoepf UJ, Renker M, Zwerner PL, O'Brien TX, et al. Coronary CT angiography: image quality, diagnostic accuracy, and potential for radiation dose reduction using a novel iterative image reconstruction technique-comparison with traditional filtered back projection. Eur Radiol. 2011;21(10):2130–8.

47. Rudin LI, Osher S, Fatemi E. Nonlinear total variation based noise removal algorithms. Phys D Nonlinear Phenom. 1992;60(1–4):259–68.

48. Tian Z, Jia X, Yuan K, Pan T, Jiang SB. Low-dose CT reconstruction via edge-preserving total variation regularization. Phys Med Biol. 2011;56(18):5949–67.

49. Hsieh J. Adaptive streak artifact reduction in computed tomography resulting from excessive x-ray photon noise. Med Phys. 1998;25(11):2139–47.

50. Zeng GL. Medical image reconstruction: a conceptual tutorial. New York: Springer; 2010. p. 1–198.

51. Hestenes MR, Stiefel E. Methods of conjugate gradients for solving linear systems. J Res Natl Bur Stand (1934). 1952;49(6):409.

52. Gould RG, Belanger B, Goldberg HI, Moss A. Objective performance measurements versus perceived image quality in intensified fluoroscopic or photospot images. Radiology. 1980;137(3):783–8.

53. Månsson LG. Methods for the evaluation of image quality: a review. Radiat Prot Dosimetry. 2000;90(1–2):89–99.

54. Juluru K, Al Khori N, He S, Kuceyeski A, Eng J. A mathematical simulation to assess variability in lung nodule size measurement associated with nodule-slice position. J Digit Imaging. 2015;28(3):373–9.

55. Svalkvist A, Håkansson M, Ullman G, Båth M. Simulation of lung nodules in chest tomosynthesis. Radiat Prot Dosimetry. 2010;139(1–3):130–9.

56. Samei E, Flynn MJ, Eyler WR. Simulation of subtle lung nodules in projection chest radiography. Radiology. 1997;202(1):117–24.

57. Tingberg A, Herrmann C, Lanhede B, Almen A, Besjakov J, Mattsson S, et al. Comparison of two methods for evaluation of the image quality of lumbar spine radiographs. Radiat Prot Dosimetry. 2000;90(1–2):165–8.

58. Dybkaer R, Jørgensen K. Measurement, value, and scale. Scand J Clin Lab Invest Suppl. 1989;194:69–76.

59. Stevens SS. On the theory of scales of measurement. Science. 1946;103(2684):677–80.

60. Svensson E. Application of a rank-invariant method to evaluate reliability of ordered categorical assessments. J Epidemiol Biostat. 1998;3(4):403–9.

61. Båth M, Månsson LG. Visual grading characteristics (VGC) analysis: a non-parametric rank-invariant statistical method for image quality evaluation. Br J Radiol. 2007;80(951):169–76.

62. Smedby Ö, Fredrikson M. Visual grading regression: analysing data from visual grading experiments with regression models. Br J Radiol. 2010;83(993):767–75.

63. Cunningham IA. Applied linear-systems theory. In: Beutel J, Kundel HL, Van Metter RL, editors. Handbook of Medical Imaging Volume 1 Physics and Psychophysics. Bellingham, Washington USA: SPIE Press; 2000. p. 79–159.

64. Richard S, Husarik DB, Yadava G, Murphy SN, Samei E. Towards task-based assessment of CT performance: system and object MTF across different reconstruction algorithms. Med Phys. 2012;39(7):4115.

65. Robins M, Solomon J, Richards T, Samei E. 3D task-transfer function representation of the signal transfer properties of low-contrast lesions in FBP- and iterative-reconstructed CT. Med Phys. 2018;45(11):4977–85.

66. Chen B, Ramirez Giraldo JC, Solomon J, Samei E. Evaluating iterative reconstruction performance in computed tomography. Med Phys. 2014;41(12):121913.

67. Li K, Tang J, Chen G-H. Statistical model based iterative reconstruction (MBIR) in clinical CT systems: Experimental assessment of noise performance. Med Phys. 2014;41(4):041906.

68. Østerås BH, Heggen KL, Pedersen HK, Andersen HK, Martinsen ACT. Can use of adaptive statistical iterative reconstruction reduce radiation dose in unenhanced head CT? an analysis of qualitative and quantitative image quality. Acta Radiol Open. 2016;5(8):205846011664583.

69. Solomon J, Samei E. Quantum noise properties of CT images with anatomical textured backgrounds across reconstruction algorithms: FBP and SAFIRE. Med Phys. 2014;41(9):091908.

70. Li K, Tang J, Chen G-H. Noise performance of statistical model based iterative reconstruction in clinical CT systems. Proc SPIE. 2014;9033:90335J.

71. Wells JR, Dobbins III JT. Frequency response and distortion properties of nonlinear image processing algorithms and the importance of imaging context. Med Phys. 2013;40(9):091906.

72. Samei E, Bakalyar D, Boedeker KL, Brady S, Fan J, Leng S, et al. Performance evaluation of computed tomography systems: summary of AAPM task group 233. Med Phys. 2019;46(11):e735–56.

73. Singh S, Kalra M, Hsieh J, Licato P. Abdominal CT : Comparison of adaptive statistical iterative and filtered back projection reconstruction techniques. Radiology. 2010;257(2):373–83.

74. Evans JD, Politte DG, Whiting BR, O'Sullivan JA, Williamson JF. Noise-resolution tradeoffs in x-ray CT imaging: a comparison of penalized alternating minimization and filtered backprojection algorithms. Med Phys. 2011;38(3):1444–58.

75. Minamishima K, Sugisawa K, Yamada Y, Jinzaki M. Quantitative and qualitative evaluation of hybrid iterative reconstruction, with and without noise power spectrum models: a phantom study. J Appl Clin Med Phys. 2018;19(3):318–25.

76. Hsieh J, Liu E, Nett B, Tang J, Thibault J-B, Sahney S. A new era of image reconstruction: TrueFidelity™ technical white paper on deep learning image reconstruction. White paper (JB68676XX). GE Healthcare. 2019.

77. Solomon J, Wilson J, Samei E. Characteristic image quality of a third generation dual-source MDCT scanner: noise, resolution, and detectability. Med Phys. 2015;42(8):4941–53.

78. Christianson O, Chen JJS, Yang Z, Saiprasad G, Dima A, Filliben JJ, et al. An improved index of image quality for task-based performance of CT iterative reconstruction across three commercial implementations. Radiology. 2015;275(3):725–34.

79. Abadi E, Segars WP, Harrawood B, Sharma S, Kapadia A, Samei E. Virtual clinical trial for quantifying the effects of beam collimation and pitch on image quality in computed tomography. J Med Imaging. 2020;7(04):1.

80. Abadi E, Segars WP, Tsui BMW, Kinahan PE, Bottenus N, Frangi AF, et al. Virtual clinical trials in medical imaging: a review. J Med Imaging. 2020;7(4):42805.

81. Smith TB, Abadi E, Solomon J, Samei E. Development, validation, and relevance of in vivo low-contrast task transfer function to estimate detectability in clinical CT images. Med Phys. 2021;48(12):7698–711.

82. Smith TB, Abadi E, Sauer TJ, Fu W, Solomon JB, Samei E. Development and validation of an automated methodology to assess perceptual in vivo noise texture in liver CT. J Med Imaging. 2021;8(5):52113.

83. Schilham A, van der Molen AF, Prokop M, de Jong HW. Overranging at multisection CT: an underestimated source of excess radiation exposure. Radiographics. 2010;30(4):1057–67.

84. Frellesen C, Stock W, Kerl JM, Lehnert T, Wichmann JL, Nau C, et al. Topogram-based automated selection of the tube potential and current in thoraco-abdominal trauma CT - a comparison to fixed kV with mAs modulation alone. Eur Radiol. 2014;24(7):1725–34.

85. Steidel J, Maier J, Sawall S, Kachelrieß M. Dose reduction potential in diagnostic single energy CT through patient-specific prefilters and a wider range of tube voltages. Med Phys. 2022;49(1):93–106.

86. Kanal KM, Stewart BK, Kolokythas O, Shuman WP. Impact of operator-selected image noise index and reconstruction slice thickness on patient radiation dose in 64-MDCT. Am J Roentgenol. 2007;189(1):219–25.

87. Solomon JB, Li X, Samei E. Relating Noise to image quality indicators in CT examinations with tube current modulation. Am J Roentgenol. 2013;200(3):592–600.

88. Leitz W, Axelsson B, Szendrö G. Computed tomography dose assessment - a practical approach. Radiat Prot Dosimetry. 1995;57(1–4):377–80.

89. Boone JM, Strauss KJ, Cody DD, McCollough CH, McNitt-Gray MF, Toth TL. Size specific dose estimates (SSDE) in pediatric and adult body CT examinations. AAPM report no 204. 2011.ISSN: 0271-7344

90. McCollough C, Bakalyar DM, Bostani M, Brady S, Boedeker K, Boone JM, et al. Use of water equivalent diameter for calculating patient size and size-specific dose estimates (SSDE) in CT. AAPM report no 220. 2014. ISSN: 0271-7344.

91. Boone JM, Strauss KJ, Hernandez AM, Hardy A, Applegate KE, Artz NS, et al. Size-specific dose estimate (SSDE) for head CT. AAPM report no 293. 2019. ISSN: 0271-7344.

92. Börjesson S, Håkansson M, Båth M, Kheddache S, Svensson S, Tingberg A, et al. A software tool for increased efficiency in observer performance studies in radiology. Radiat Prot Dosimetry. 2005;114(1–3):45–52.

93. Håkansson M, Svensson S, Zachrisson S, Svalkvist A, Båth M, Månsson LG. ViewDEX: an efficient and easy-to-use software for observer performance studies. Radiat Prot Dosimetry. 2010;139(1–3):42–51.

94. Svalkvist A, Svensson S, Håkansson M, Båth M, Månsson LG. ViewDEX: a status report. Radiat Prot Dosimetry. 2016;169(1–4):38–45.

95. Svalkvist A, Svensson S, Hagberg T, Båth M. Viewdex 3.0 - recent development of a software application facilitating assessment of image quality and observer performance. Radiat Prot Dosimetry. 2021;195(3–4):372–7.

96. Ledenius K, Stålhammar F, Wiklund L-M, Fredriksson C, Forsberg A, Thilander-Klang A. Evaluation of image-enhanced paediatric computed tomography brain examinations. Radiat Prot Dosimetry. 2010;139(1):287–92.

97. Ledenius K. Optimization of paediatric CT examinations - an approach to minimize absorbed dose to patients with regard to image quality and observer variability. PhD thesis. University of Gothenburg; 2011. Available from: http://hdl.handle.net/2077/24021

98. Svensson E. A coefficient of agreement adjusted for bias in paired ordered categorical data. Biometrical J. 1997;39(6):643.

99. Ledenius K, Svensson E, Stålhammar F, Wiklund LM, Thilander-Klang A. A method to analyse observer disagreement in visual grading studies: example of assessed image quality in paediatric cerebral multidetector CT images. Br J Radiol. 2010;83(991):604–11.

100. Svensson E. Statistisk metod för parade ordinaldata. Läkartidningen. 2007;104(8):596–601.

101. Dainty JC, Shaw R. Image science : principles, analysis and evaluation of photographic-type imaging processes. London: Academic Press; 1974.

102. Kim KH, Shin DS, Kang SW, Kang SH, Kim TH, Chung JB, et al. Four-dimensional inverse-geometry computed tomography: a preliminary study. Phys Med Biol. 2021;66(6):65028.

103. Lim CG, Park SJ, Ahn CB. Tile-net for undersampled cardiovascular CINE magnetic resonance imaging. Magn Reson Imaging. 2021;84:27–34.

104. Gao F, Wu M. Deep learning-based denoised MRI images for correlation analysis between lumbar facet joint and lumbar disc herniation in spine surgery. J Healthc Eng. 2021;2021 Article ID 9687591:1-7.

105. Zhou Wang, Bovik, Ligang Lu. Why is image quality assessment so difficult? 2002 IEEE International Conference on Acoustics, Speech, and Signal Processing. 2002;IV:3313–16.

106. Wang Z, Bovik AC, Sheikh HR, Simoncelli EP. Image quality assessment: from error visibility to structural similarity. IEEE Trans Image Process. 2004;13(4):600–12.

107. Sheikh HR, Bovik AC. Image information and visual quality. IEEE Trans Image Process. 2006;15(2):430–44.

108. Larson EC, Chandler DM. Most apparent distortion: full-reference image quality assessment and the role of strategy. J Electron Imaging. 2010;19(1):011006.

109. Gonzúlez DA, Mccall JC. Design of filters to reduce harmonic distortion in industrial power systems. IEEE Trans Ind Appl. 1987;IA-23(3):504–11.

110. Hwang GY, Kim H-G, Hwang SM, Kang BS. Analysis of harmonic distortion due to uneven magnetic field in a micro-speaker used for mobile phones. INTERMAG Eur 2002 - IEEE Int Magn Conf. 2002;38(5):2376–8.

111. Shmilovitz D. On the definition of total harmonic distortion and its effect on measurement interpretation. IEEE Trans Power Deliv. 2005;20(1):526–8.

112. van Aarle W, Palenstijn WJ, De Beenhouwer J, Altantzis T, Bals S, Batenburg KJ, et al. The ASTRA toolbox: a platform for advanced algorithm development in electron tomography. Ultramicroscopy. 2015;157(2015):35–47.

113. van Aarle W, Palenstijn WJ, Cant J, Janssens E, Bleichrodt F, Dabravolski A, et al. Fast and flexible X-ray tomography using the ASTRA toolbox. Opt Express. 2016;24(22):25129.

114. Palenstijn WJ, Batenburg KJ, Sijbers J. Performance improvements for iterative electron tomography reconstruction using graphics processing units (GPUs). J Struct Biol. 2011;176(2):250–3.

115. Chatzaraki V, Kubik-Huch RA, Thali M, Niemann T. Quantifying image quality in chest computed tomography angiography: evaluation of different contrast-to-noise ratio measurement methods. Acta radiol. 2021;63(10):1353-62

116. Hubbell JH, Seltzer SM. NIST: X-ray mass attenuation coefficients. Physical Reference Data. 1996. Available from: https://www.nist.gov/pml/x-ray-mass-attenuation-coefficients

117. Cheong KH, Yoon JW, Park S, Hwang T, Kang SK, Koo T, et al. Enhancement of megavoltage electronic portal images for markerless tumor tracking. J Appl Clin Med Phys. 2018;19(5):398–406.

118. Kilic K, Erbas G, Guryildirim M, Arac M, Ilgit E, Coskun B. Lowering the dose in head CT using adaptive statistical iterative reconstruction. Am J Neuroradiol. 2011;32(9):1578–82.

119. Komlosi P, Zhang Y, Leiva-Salinas C, Ornan D, Patrie JT, Xin W, et al. Adaptive statistical iterative reconstruction reduces patient radiation dose in neuroradiology CT studies. Neuroradiology. 2014;56(3):187–93.

120. Guziński M, Waszczuk Ł, Sąsiadek MJ. Head CT: Image quality improvement of posterior fossa and radiation dose reduction with ASiR - comparative studies of CT head examinations. Eur Radiol. 2016;26(10):3691–6.

121. McKnight CD, Watcharotone K, Ibrahim M, Christodoulou E, Baer AH, Parmar HA. Adaptive statistical iterative reconstruction: reducing dose while preserving image quality in the pediatric head CT examination. Pediatr Radiol. 2014;44(8):997–1003.

122. Kilic K, Erbas G, Guryildirim M, Konus OL, Arac M, Ilgit E, et al. Quantitative and qualitative comparison of standard-dose and low-dose pediatric head computed tomography: a retrospective study assessing the effect of adaptive statistical iterative reconstruction. J Comput Assist Tomogr. 2013;37(3):377–81.

123. Kataria B, Althén JN, Smedby Ö, Sökjer H, Sandborg M. Assessment of image quality in abdominal CT : potential dose reduction with model-based iterative reconstruction. Eur Radiol. 2018;28(6):2464–73.

124. Silva AC, Lawder HJ, Hara A, Kujak J, Pavlicek W. Innovations in CT dose reduction strategy: application of the adaptive statistical iterative reconstruction algorithm. Am J Roentgenol. 2010;194(1):191–9.

125. Sugisawa K, Ichikawa K, Urikura A, Minamishima K, Masuda S, Hoshino T, et al. Spatial resolution compensation by adjusting the reconstruction kernels for iterative reconstruction images of computed tomography. Phys Medica. 2020;74:47–55.

126. Akagi M, Nakamura Y, Higaki T, Narita K, Honda Y, Zhou J, et al. Deep learning reconstruction improves image quality of abdominal ultra-high-resolution CT. Eur Radiol. 2019;29(11):6163–71.

127. Sun J, Li H, Li J, Yu T, Li M, Zhou Z, et al. Improving the image quality of pediatric chest CT angiography with low radiation dose and contrast volume using deep learning image reconstruction. Quant Imaging Med Surg. 2021;11(7):3051–8.

128. Arndt C, Güttler F, Heinrich A, Bürckenmeyer F, Diamantis I, Teichgräber U. Deep learning CT image reconstruction in clinical practice. Rofo. 2021;193(3):252–61.

129. Nakamura Y, Higaki T, Tatsugami F, Zhou J, Yu Z, Akino N, et al. Deep learning–based CT image reconstruction: Initial Evaluation Targeting Hypovascular Hepatic Metastases. Radiol Artif Intell. 2019;1(6):e180011.

130. Benz DC, Benetos G, Rampidis G, von Felten E, Bakula A, Sustar A, et al. Validation of deep-learning image reconstruction for coronary computed tomography angiography: impact on noise, image quality and diagnostic accuracy. J Cardiovasc Comput Tomogr. 2020;14(5):444–51.

131. Solomon J, Samei E. Quantum noise properties of CT images with anatomical textured backgrounds across reconstruction algorithms: FBP and SAFIRE. Med Phys. 2014;41(9):91908.

132. Barca P, Giannelli M, Evelina M, Caramella D. Computed tomography imaging with the adaptive statistical iterative reconstruction (ASIR) algorithm : dependence of image quality on the blending level of reconstruction. Australas Phys Eng Sci Med. 2018;41(2):463–73.

133. Greffier J, Hamard A, Pereira F, Barrau C, Pasquier H, Beregi JP, et al. Image quality and dose reduction opportunity of deep learning image reconstruction algorithm for CT: a phantom study. Eur Radiol. 2020;30(7):3951–9.

134. Greffier J, Dabli D, Frandon J, Hamard A, Belaouni A, Akessoul P, et al. Comparison of two versions of a deep learning image reconstruction algorithm on CT image quality and dose reduction: a phantom study. Med Phys. 2021;48(10),5743–55

135. Willemink MJ, Noël PB. The evolution of image reconstruction for CT—from filtered back projection to artificial intelligence. Eur Radiol. 2019;29(5):2185–95.

136. Khawaja RDA, Singh S, Otrakji A, Padole A, Lim R, Nimkin K, et al. Dose reduction in pediatric abdominal CT: use of iterative reconstruction techniques across different CT platforms. Pediatr Radiol. 2015;45(7):1046–55.

137. Cao L, Liu X, Li J, Qu T, Chen L, Cheng Y, et al. A study of using a deep learning image reconstruction to improve the image quality of extremely low-dose contrast-enhanced abdominal CT for patients with hepatic lesions. Br J Radiol. 2021;94(1118):20201086.

138. Jiang B, Li N, Shi X, Zhang S, Li J, de Bock GH, et al. Deep learning reconstruction shows better lung nodule detection for ultra–low-dose chest CT. Radiology. 2022;303(1):202–12.

'… For there is a man
whose labour is in wisdom,
and in knowledge, and in equity;
yet to a man that hath not laboured
therein shall he leave it for his portion…'

Ecclesiastes 2:18-26 KJV